Hindawi Publishing Corporation
EURASIP Journal on Image and Video Processing
Volume 2010, Article ID 624271, 24 pages
doi:10.1155/2010/624271

Research Article

Design of Vertically Aligned Binocular Omnistereo Vision Sensor

Yi-ping Tang,[1] Qing Wang,[2] Ming-li Zong,[2] Jun Jiang,[2] and Yi-hua Zhu[2]

[1] *College of Information Engineering, Zhejiang University of Technology, Hangzhou 310023, China*
[2] *College of Computer Science and Technology, Zhejiang University of Technology, Hangzhou 310023, China*

Correspondence should be addressed to Qing Wang, wangqing2688@126.com

Received 30 November 2009; Revised 13 May 2010; Accepted 24 August 2010

Academic Editor: Pascal Frossard

Catadioptric omnidirectional vision sensor (ODVS) with a fixed single view point is a fast and reliable single panoramic visual information acquisition equipment. This paper presents a new type of binocular stereo ODVS which composes of two ODVS with the same parameters. The single view point of each ODVS is fixed on the same axis with face-to-face, back-to-back, and face-to-back configuration; the single view point design is implemented by catadioptric technology such as the hyperboloid, constant angular resolution, and constant vertical resolution. The catadioptric mirror design uses the method of increasing the resolution of the view field and the scope of the image in the vertical direction. The binocular stereo ODVS arranged in vertical is designed spherical, cylindrical surfaces and rectangular plane coordinate system for 3D calculations. Using the collinearity of two view points, the binocular stereo ODVS is able to easily align the azimuth, while the camera calibration, feature points match, and other cumbersome steps have been simplified. The experiment results show that the proposed design of binocular stereo ODVS can solve the epipolar constraint problems effectively, match three-dimensional image feature points rapidly, and reduce the complexity of three-dimensional measurement considerably.

1. Introduction

Designing vision sensors is critical for developing, simplifying, and improving several applications in computer vision and other areas. Some traditional problems like scene representation, surveillance, and mobile robot navigation are found to be conveniently tackled by using different sensors, which leads to much more effort made in researching and developing omnidirectional vision systems, that is, systems capable of capturing objects in all directions [1–11].

An omnidirectional image has a 360-degree view around a viewpoint, and in its most common form, it can be presented in a cylindrical or spherical surface around the viewpoint. Usually, an omnidirectional image can be obtained either by an image mosaicing technique or by an omnidirectional camera. An omnidirectional camera is widely used in practice, since it is able to capture real-time three-dimensional space of the scene information and can avoid the complexities arising from dealing with image mosaicing. In this paper, kinds of vertically aligned binocular (V-binocular) omnistereo, which are composed of a pair of hyperbolic-shaped mirrors, a constant angular resolution mirror, or a constant vertical resolution mirror, are investigated. Moreover, critical issues on omnidirectional stereo imaging, structural design, epipolar geometry, and depth accuracy are discussed and analyzed.

The binocular stereoscopic 3D measurement and 3D reconstruction technology based on computer vision are new technology with great potential in development and practice, which can be widely used in such areas as industrial inspection, military reconnaissance, geographical surveying, medical cosmetic surgery, bone orthopaedics, cultural reproduction, criminal evidence, security identification, air navigation, robot vision, virtual reality, animated films, games, and so on. Besides, it has become a hot spot in the computer vision research community [12–14].

Stereo vision is based on binocular parallax principle of the human eyes [15–18] to perceive 3D information, which imitates the method used by human being to apperceive distance in binocular clues. Distance between objects is obtained from binocular parallax of the two images, respectively, captured by two eyes for the same object, which makes a stereo image vivid as depth information is include in the image. There are two main shortcomings in the stereo

vision technology: (1) camera calibration, matching, and reconstruction are still not resolved perfectly, and (2) it is not able to capture panoramic view and to make people feel being in the scene personally since it is object-centered and with narrow-view; that is, it only captures a small part of the scene. Fortunately, the second shortcoming is overcome by the ODVS technology [19], a viewer-centered technology, which eliminates the narrow-view problem so that a panoramic view is gained.

Currently, there exist some challenges in binocular stereo vision, which belong to vision ill-posed problems including camera calibration, feature extraction, stereo image matching, and so forth. For calibration, it is well known that upon camera calibration is set, focal length is fixed, which leads the depth of the captured image to be unchanged and only within limited range. In other words, camera calibration is needed to be reset if we need to change the depth. Another disadvantage of calibration is that changing parameters are avoided in a variety of movement in 3D visual measurement system [20–22]. These disadvantages limit the application of the binocular stereo vision. Additionally, disadvantages in feature extraction and stereo image matching are mainly as follows. The processes of various shapes from X incur coordinate transformation to be performed many times, which produces extraneous calculation and makes it impossible to conduct real-time processing. Besides, there exists a high mismatching probability in matching corresponding points, yielding high rate of matching errors and reducing matching accuracy. Nowadays, 3D visual matching is a typical ill-posed calculation and it is difficult to get 3D match unambiguously and accurately [23].

Advances in ODVS technology in recent years provide a new solution for acquiring a panoramic picture of the scenes in real time [24]. The feature of ODVS with wide range of vision can be used to compress the information of the hemispheric vision into an image including a great volume of information. On the other hand, ODVS can be freely placed to get a scene image. ODVS establishes a technical foundation for building a 3D visual sensing measurement system.

There are many types of omnidirectional vision system, which based on rotating cameras, fish-eye lens or mirrors. This paper is mainly concerned with the omnidirectional vision systems combining cameras with mirrors, normally referred as catadioptric systems in the optics domain, especially in what concerns the mirror profile design. The shape of the mirror determines the image formation model of a catadioptric omnidirectional camera. In some cases, one can design the shape of the mirror in such a way that certain world-to-image geometric properties are preserved, referred as linear projection properties.

2. Motivation of the Research

The use of robots is an attractive option in places where human intervention is too expensive or hazardous. Robots have to explore the environment using a combination of their onboard sensors and eventually process the obtained data and transform it in useful information for further decisions or for human interpretation. Therefore, it is critical to provide the robot with a model of the real scene or with the ability to build such a model by itself. Our research is motivated by the construction of a visual and nonintrusive environment model.

The omnidirectional vision enhances the field of view of traditional cameras by using special optics and combinations of lenses and mirrors. Besides the obvious advantages offered by a large field of view, in robot navigation the necessity of employing omnidirectional sensors also stems from a well-known problem in computer vision: the motion estimation algorithms may mistake a small pure translation of the camera for a small rotation, and the possibility of error increases if the field of view is narrow or the depth variations in the scene are small. An omnidirectional sensor can eliminate this error since it receives more information for the

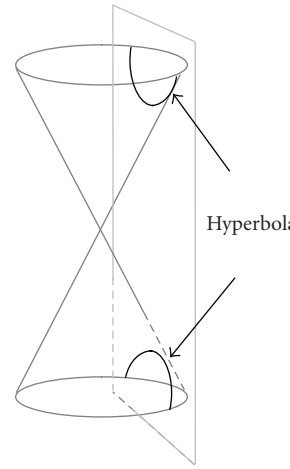

Figure 1: The hyperbola formed by a plane intersecting both nappes of a cone [25].

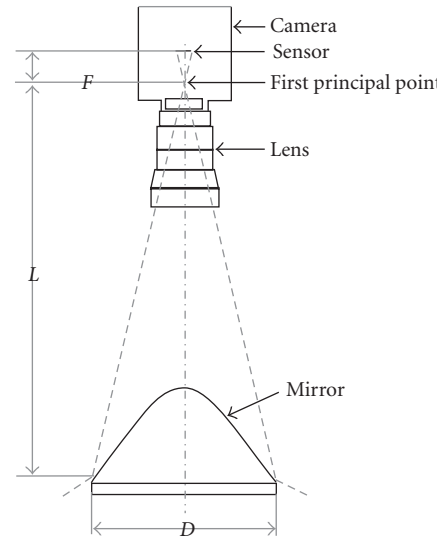

Figure 2: Omnidirectional camera and lens configuration [26].

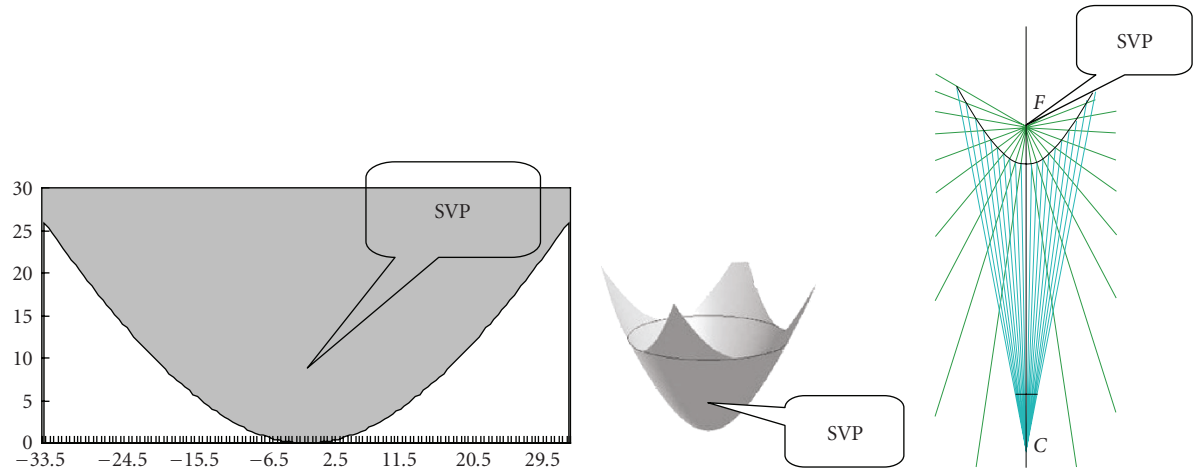

Figure 3: Hyperbolic-shaped mirror. (a) Hyperbolic profile with the parameters $a = 51.96$ and $b = 30$. The dot represents the focal point of the mirror, that is, the SVP of the sensor. (b) The same hyperbolic mirror represented in 3D space. (c) Isotropic of hyperbolic mirror.

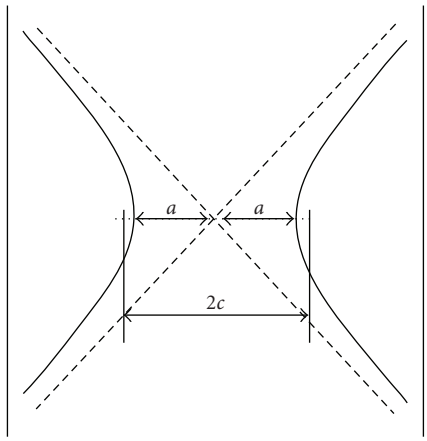

Figure 4: The relat ion between the parameters a and c and the hyperbolic profile [25].

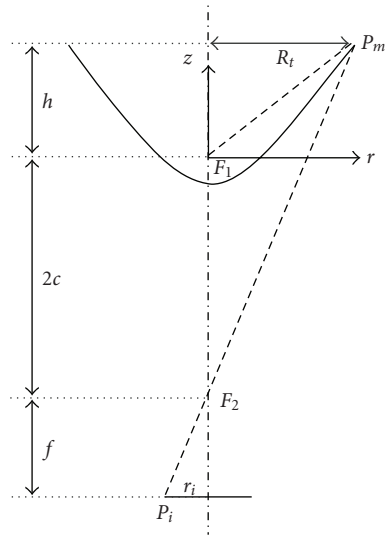

Figure 5: The relation between the size of the sensor and the intrinsic parameters of the omnidirectional camera.

same movement of the camera than the one obtained by a reduced field of view sensor.

According to different practical application cases, three kinds of coordinate system on vertically aligned binocular omnistereo vision sensor are proposed, namely, spherical surface sensing type, cylindrical surface sensing type, and orthogonal coordinates sensing type. For spherical surface sensing type, it is desired to ensure uniform angular resolution as if the camera had a spherical geometry. This sensor has interesting properties (e.g., ego-motion estimation). For cylindrical surface sensing type, this design constraint aims to the goal that objects at a (prespecified) fixed distance from the camera's optical axis will always have the same size in the image, independent of its vertical coordinates. Orthogonal coordinates sensing type ensures that the ground plane is imaged under a scaled Euclidean transformation.

It is significant to build a uniform coordinate system for 3D stereo vision so that ill-posed calculation is avoided. Motivated by this, we investigate designing binocular stereo ODVS and build a uniform spherical coordinate system, in which computational geometry is used in object depth calculation, the 3D visual matching, and the 3D image reconstruction. The main contributions of this paper are as follows: (1) two omnidirectional vision equipment are seamlessly combined to capture objects without shelter; (2) the overlay vision area in the designed sensors (which is generated from visual fields of two ODVSs being combined in back-to-back configuration for spherical surface 3D stereo vision, face-to-face configuration for cylindrical surface 3D stereo vision, or face-to-back configuration for photogrammetry), makes it possible for a binocular stereo ODVS to perceive, match, and capture stereoscopic images at the same

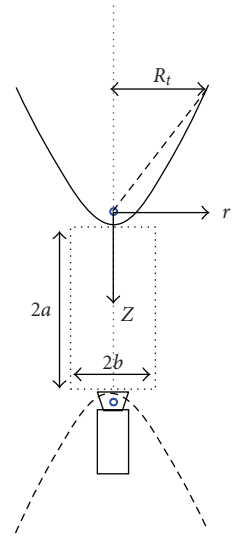

Figure 6: High vertical FOV hyperbolic mirror suitable for binocular omnistereo. The parameters of the mirror are $a = 19$, $b = 10$, and $R_t = 25$. The vertical FOV above the horizon is of 49.8 degrees.

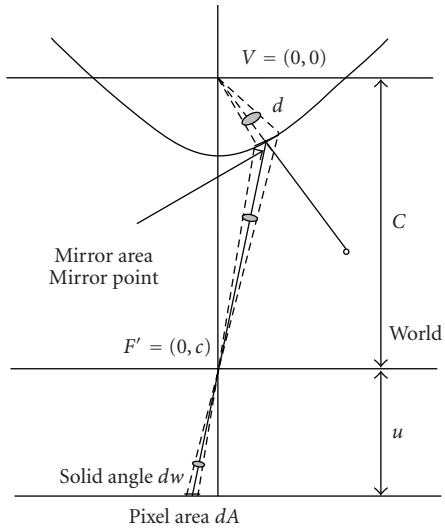

Figure 7: The geometry to derive spatial resolution of catadioptric system.

time; (3) a uniform Gaussian sphere coordinate system is presented for image capturing, 3D matching, and 3D image reconstruction so that computing models are simplified. All the above contributions together with features of ODVSs simplify the camera calibration and feature point matching.

3. Design of Catadioptric Cameras

Catadioptric cameras act like analog computers performing transformations from 3D space to the 2D image plane through the combination of mirrors and lenses. The mirrors used in catadioptric cameras must cover the full azimuthal FOV (Field of View) and thus are symmetric revolution

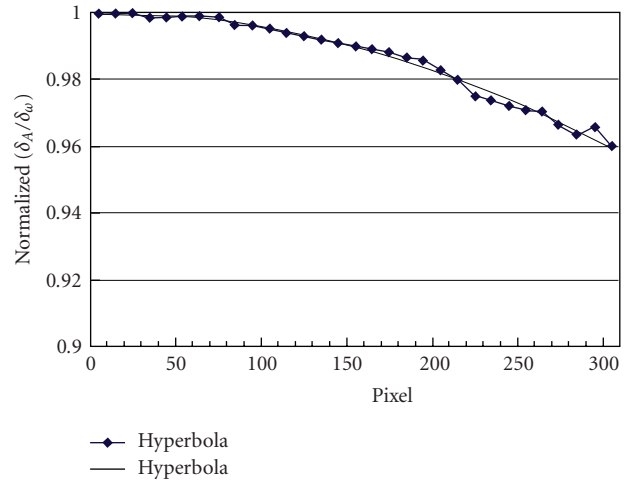

Figure 8: Resolution of ODVS having a perspective camera and an hyperbolic mirror where a pinhole located at the coordinate system origin $d = 0$.

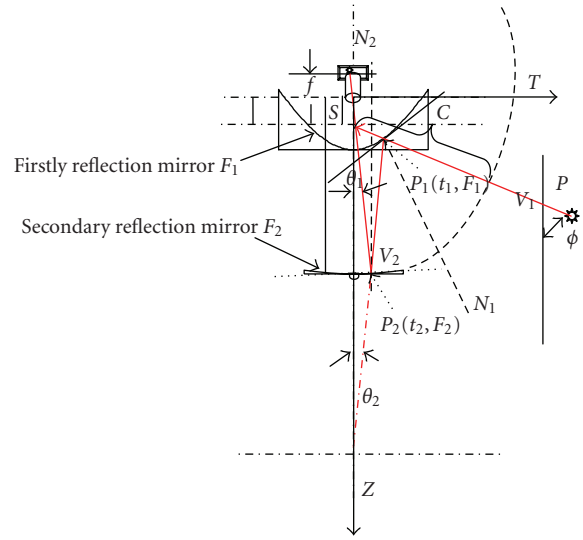

Figure 9: Imaging principle of catadioptric of constant angular resolution.

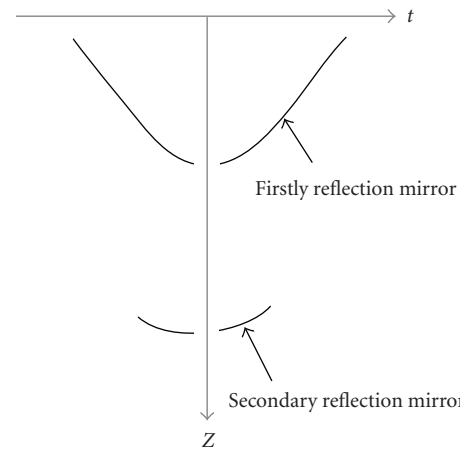

Figure 10: Reflectors curvilinear figure solution.

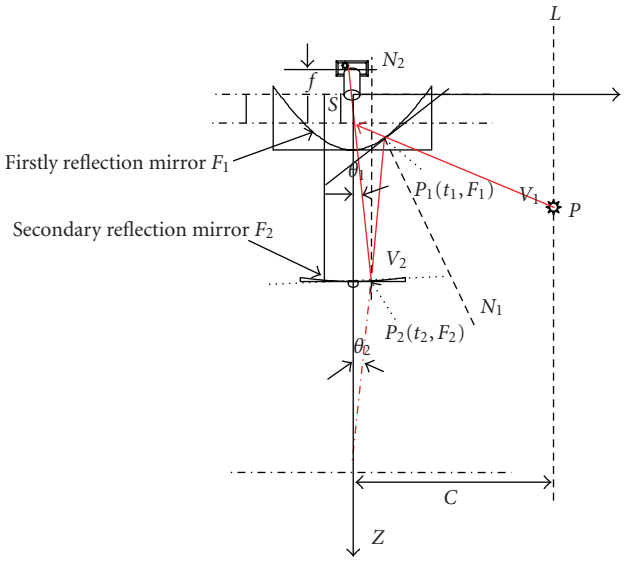

Figure 11: Imaging principle of catadioptric of constant vertical resolution.

shapes, usually with conic profile. The cameras are first classified with respect to the SVP (Single View Point) property and then classified according to the mirror shapes used in their fabrication. We focus on the omnidirectional cameras with depth perception capabilities that are highlighted among the other catadioptric configurations. Finally, we present the epipolar geometry for catadioptric cameras.

Catadioptrics are combinations of mirrors and lenses, which arranged carefully to obtain a wider field of view than the one obtained by conventional cameras. In catadioptric systems, the image suffers a transformation due to the reflection in the mirror. This alteration of the original image depends on the mirror shape. Therefore, a special care was given to the study of the mirror optical properties. There are several ways to approach the design of a catadioptric sensor. One method is to start with a given camera and find out the mirror shape that best fits its constraints. Another technique is to start from a given set of required performances such as field of view, resolution, defocus blur, and image transformation constraints and so forth, then search for the optimal catadioptric sensor. In both cases, a compulsory step is to study the properties of the reflecting surfaces.

Most of the mirrors considered in the next sections are surfaces of revolution, that is, 3D shapes generated by rotating a two-dimensional curve about an axis. The resulting surface therefore always has azimuthally symmetry. Moreover, the rotated curves are conic sections, that is, curves generated by the intersections of a plane with one or two nappes of a cone as shown in Figure 1. For instance, a plane perpendicular to the axis of the cone produces a circle while the curve produced by a plane intersecting both nappes is a hyperbola. Rotating these curves about their axis of symmetry, a sphere and a hyperboloid are obtained.

An early use of a catadioptric for a real application was proposed by Rees in 1970 [Rees, 1970]. He invented a panoramic television camera based on a convex, hyperbolic-shaped mirror shown in Figure 2. Twenty years later, once again researchers focused their attention on the possibilities offered by the catadioptric systems, mostly in the field of robotics vision. In 1990, the Japanese team from Mitsubishi Electric Corporation lead by Yagi [Yagi and Kawato, 1990] studied the panoramic scenes generated using a conic mirror-based sensor. The sensor, named COPIS 2, was used to generating the environmental map of an indoor scene from a mobile robot. The conic mirror shape was also used, in 1995, by the researchers from the University of Picardie Jules Verne, lead by Mouaddib. Their robot was provided with an omnidirectional sensor, baptized SYCLOP 3, which captures 360-degree images at each frame and was used for navigation and localization in the 3D space [Pegard and Mouaddib, 1996].

Since the mid-1990s of last century, omnidirectional vision and its knowledge base have increasingly attracted attention with the increase in the number of researchers involved in omnidirectional cameras. Accordingly, new mathematical models for catadioptric projection and consequently better performing catadioptric sensors have appeared.

Central catadioptric sensors are the class of these devices having a single effective viewpoint [25]. The reason for a single viewpoint is from the requirement for the generation of pure perspective images from the sensed images. This requirement ensures that the visual sensor only measures the intensity of light passing through a projection center. It is highly desirable that the omnidirectional sensor have a single effective center of projection, that is, a single point through which all the chief rays of the imaging system pass. This center of projection serves as the effective pinhole (or viewpoint) of the omnidirectional sensor. Since all scene points are "seen" from this single viewpoint, pure perspective images that are distortion free (like those seen from a traditional imaging system) can be constructed via suitable image transformation.

The omnidirectional image has different features from the image captured by standard camera. Vertical resolution of the transformed image has usually nonuniform distribution. The circle which covers the highest number of pixels is projected from the border of the mirror, which means that the transformed image resolution is decreasing towards the mirror center. If the image is presented to a human, a perspective/panoramic image is needed so as not to appear distorted. When we want to further process the image, other issues should be carefully considered, such as spatial resolution, sensor size, and ease of mapping between the omnidirectional images and the scene.

The parabolic-shaped mirror is a solution of the SVP constraint in a limiting case which corresponds to orthographic projection. The parabolic mirror works in the same way as the parabolic antenna: the incoming rays pass through the focal point and reflected parallel to the rotating axis of the parabola. Therefore, a parabolic mirror should be used in conjunction with an orthographic camera. A perspective camera can also be used if it is placed very far from the mirror so that the reflected rays can be approximated as

Table 1: ODVS composing vertically aligned binocular omnistereo.

Type	Construction	Depth	Resolution	SVP	Isotropic	VFOV
Single camera with single mirror	Hyperbolic-shaped mirror	no	change	yes	yes	yes
Single camera with two mirrors	Constant angular resolution mirror	no	Constant in spherical surface	yes	yes	yes
	Constant vertical resolution mirror	no	Constant in cylindrical surface	yes	yes	yes

Table 2: Experement resluts of measuring depth between view point and object from 30 cm to 250 cm using V-binocular ODVS with face-toface configuration in Figure 15(b).

Actual depth (cm)	Up image plane coordinates C_{up} (x_1, y_1)	Angle of incidence ϕ_1 (degree)	Down image plane coordinates C_{down} (x_2, y_2)	Angle of incidence ϕ_2 (degree)	Depth estimation (cm)	Error ratio (%)
30.00	300,34	57.84	300,40	55.82	31.04	3.47
40.00	301,39	65.04	301,54	62.70	41.36	3.39
50.00	301,59	69.54	301,66	68.21	52.52	5.03
60.00	301,57	72.96	301,72	70.84	62.08	3.47
70.00	298,62	75.03	298,79	73.80	72.74	3.91
80.00	300,67	77.04	300,83	75.44	82.85	3.56
90.00	299,70	78.22	299,87	77.04	92.52	2.80
100.00	299,73	79.38	299,90	78.22	102.46	2.46
110.00	300,76	80.52	300,92	78.99	112.27	2.06
120.00	299,78	81.27	299,93	79.38	118.97	−0.86
130.00	298,80	82.01	298,94	79.76	126.42	−2.75
140.00	302,81	82.37	302,99	81.64	144.47	3.20
150.00	298,82	82.74	298,99	81.64	147.89	−1.40
160.00	299,83	83.10	299,101	82.37	159.21	−0.49
170.00	298,83	83.10	298,102	82.74	163.36	−3.91
180.00	300,84	83.46	300,103	83.10	172.24	−4.31
190.00	301,86	84.18	301,103	83.10	182.00	−4.21
200.00	299,87	84.53	299,104	83.46	192.93	−3.54
210.00	298,87	84.53	298,106	84.18	205.24	−2.27
220.00	299,88	84.88	299,107	84.53	219.04	−0.44
230.00	298,88	84.88	298,107	84.53	219.07	−4.77
240.00	299,89	85.23	299,109	85.23	243.37	1.40
250.00	298,89	85.23	298,109	85.23	243.37	−2.65

Table 3: Experement resluts of measuring depth between view point and object from 100 cm to 1100 cm using V-binocular ODVS with face-to-face configuration in Figure 15(b).

Actual depth (cm)	Up image plane coordinates C_{up} (x_1, y_1)	Angle of incidence ϕ_1 (degree)	Down image plane coordinates C_{down} (x_2, y_2)	Angle of incidence ϕ_2 (degree)	Depth estimation (cm)	Error ratio (%)
100.00	299,83	79.38	299,90	78.22	102.46	2.46
200.00	299,87	84.53	299,104	83.46	192.93	−3.54
300.00	299,91	85.93	299,110	85.58	273.4	−8.86
400.00	301,100	88.96	301,113	86.62	425.37	6.34
500.00	298,103	89.93	298,110	85.58	480.42	−3.92
600.00	302,104	90.25	302,111	85.93	608.52	1.42
700.00	300,104	90.25	300,112	86.27	668.99	−4.43
800.00	300,106	90.89	300,112	86.27	819.20	2.40
900.00	302,104	90.25	302,114	86.96	832.99	−7.45
1000.00	301,104	90.25	301,116	87.63	1099.15	9.91
1100.00	300,107	91.21	300,114	86.96	1264.88	14.99

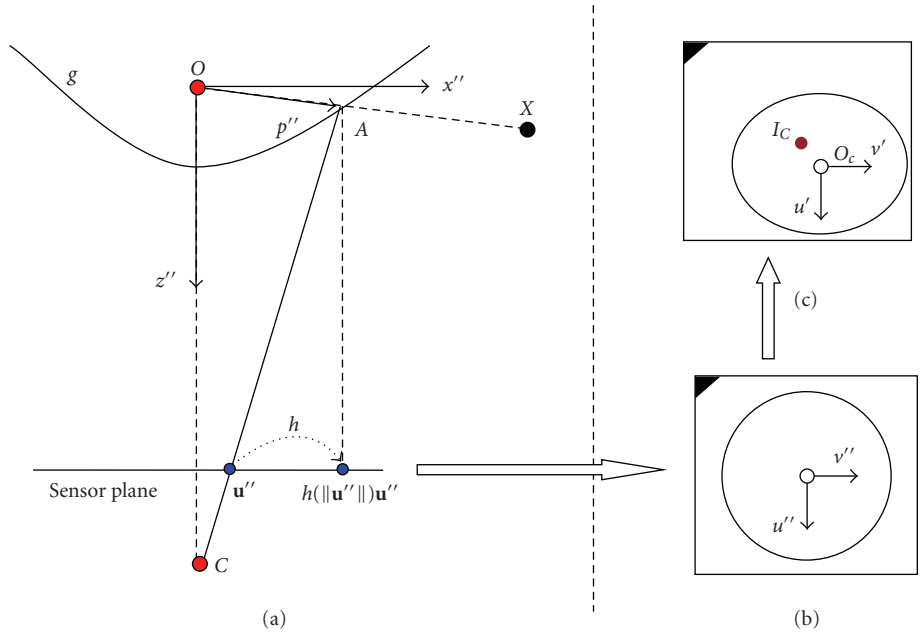

Figure 12: Single viewpoint catadioptric camera imaging model (a) perspective of the imaging process, (b) sensor plane, and (c) image plane.

Table 4: Experement resluts of measuring depth between view point and object from 30 cm to 250 cm using V-binocular ODVS with back-to-back configuration in Figure 16(b).

Actual depth (cm)	Up image plane coordinates C_{up} (x_1, y_1)	Angle of incidence ϕ_1 (degree)	Down image plane coordinates C_{down} (x_2, y_2)	Angle of incidence ϕ_2 (degree)	Depth estimation (cm)	Error ratio (%)
30.00	618,47	98.81	618,151	98.26	33.08	10.28
40.00	618,52	97.43	618,143	96.02	42.25	5.63
50.00	616,57	96.02	616,138	94.56	54.05	8.11
60.00	618,60	95.15	618,136	93.97	62.99	4.98
70.00	617,62	94.56	617,134	93.37	72.73	3.91
80.00	616,62	94.56	616,131	92.45	82.54	3.18
90.00	616,64	93.97	616,130	92.14	95.21	5.79
100.00	617,66	93.37	617,129	91.83	100.50	0.50
110.00	617,66	93.37	617,129	91.83	112.64	2.40
120.00	616,66	93.37	616,128	91.52	120.16	0.14
130.00	617,67	93.06	617,128	91.52	128.50	−1.15
140.00	616,67	93.06	616,127	91.21	138.44	−1.12
150.00	618,67	93.06	618,127	91.21	138.44	−7.71
160.00	619,68	92.76	619,127	91.21	149.68	−6.45
170.00	616,69	92.45	616,127	91.21	162.99	−4.12
180.00	619,69	92.45	619,126	90.89	179.38	−0.35
190.00	616,69	92.45	616,126	90.89	179.38	−5.59
200.00	617,70	92.14	617,126	90.89	198.92	−0.54
210.00	619,70	92.14	619,126	90.89	198.92	−5.28
220.00	618,71	91.83	618,124	90.25	298.44	35.65
230.00	617,71	91.83	617,124	90.25	298.44	29.76
240.00	616,71	91.83	616,124	90.25	298.44	24.35
250.00	617,71	91.83	617,124	90.25	298.44	19.38

Table 5: Experement resluts of measuring depth between view point and object from 100 cm to 1100 cm using V-binocular ODVS with back-to-back configuration in Figure 16(b).

Actual depth (cm)	Up image plane coordinates C_{up} (x_1, y_1)	Angle of incidence ϕ_1 (degree)	Down image plane coordinates C_{down} (x_2, y_2)	Angle of incidence ϕ_2 (degree)	Depth estimation (cm)	Error ratio (%)
100.00	617,67	93.37	617,129	91.83	100.50	0.01
200.00	617,70	92.14	617,126	90.89	198.92	−0.54
300.00	617,71	91.87	617,123	89.93	359.08	19.69
400.00	617,72	91.40	617,120	88.96	462.75	15.69
500.00	617,73	91.12	617,118	88.30	645.85	29.17
600.00	617,70	92.14	617,124	90.25	969.43	61.57
700.00	617,71	91.83	617,124	90.25	1113.63	59.09
800.00	618,71	91.83	618,123	89.93	1316.21	64.53
900.00	617,71	91.83	617,129	91.83	1610.93	78.99
1000.00	618,72	91.52	618,122	89.61	2055.70	105.57
1100.00	617,72	91.52	617,125	90.72	2884.77	162.25

Table 6: Experement resluts of measuring depth between view point and object from 30 cm to 250 cm using V-binocular ODVS with face-to-back configuration in Figure 17(b).

Actual depth (cm)	Up image plane coordinates C_{up} (x_1, y_1)	Angle of incidence ϕ_1 (degree)	Down image plane coordinates C_{down} (x_2, y_2)	Angle of incidence ϕ_2 (degree)	Depth estimation (cm)	Error ratio (%)
30.00	134,79	73.80	134,163	106.29	32.09	6.97
40.00	132,88	77.44	132,149	102.95	41.29	3.22
50.00	134,94	79.76	134,139	100.41	51.33	2.65
60.00	135,98	81.27	135,133	98.81	60.60	0.99
70.00	133,99	82.37	133,129	97.71	69.43	−0.81
80.00	132,103	83.10	132,126	96.87	77.42	−3.22
90.00	132,106	84.18	132,123	96.02	90.15	0.17
100.00	134,107	84.53	134,120	95.15	100.60	0.60
110.00	134,109	85.23	134,119	94.86	111.07	0.97
120.00	132,110	85.58	132,118	94.56	119.06	−0.78
130.00	135,111	85.93	135,117	93.97	133.05	2.34
140.00	134,112	86.27	134,117	93.97	139.02	−0.70
150.00	133,112	86.27	133,114	93.37	150.84	0.56
160.00	134,113	86.62	134,114	93.37	158.51	−0.93
170.00	133,113	86.62	133,113	93.06	165.98	−2.37
180.00	132,114	86.96	132,113	93.06	175.25	−2.64
190.00	134,114	86.96	134,112	92.76	184.47	−2.91
200.00	132,115	87.29	132,112	92.76	195.92	−2.04
210.00	132,115	87.29	132,111	92.45	207.59	−1.15
220.00	132,116	87.63	132,111	92.45	222.10	0.95
230.00	135,116	87.63	135,110	92.14	237.30	3.18
240.00	133,116	87.63	133,110	92.14	237.30	−1.12
250.00	134,116	87.63	134,109	91.83	254.85	1.94

parallel. Obviously, this solution would provide unacceptable low resolution and has no practical value for binocular omnistereo.

In summary, the great interest generated by catadioptric is due to their specific advantages when compared to other omnidirectional systems, especially VFOV, the price, and the compactness.

Table 7: Experement resluts of measuring depth between view point and object from 100 cm to 1100 cm using V-binocular ODVS with face-to-back configuration in Figure 17(b).

Actual depth (cm)	Up image plane coordinates C_{up} (x_1, y_1)	Angle of incidence ϕ_1 (degree)	Down image plane coordinates C_{down} (x_2, y_2)	Angle of incidence ϕ_2 (degree)	Depth estimation (cm)	Error ratio (%)
100.00	134,107	84.53	134,120	95.15	100.60	0.60
200.00	132,115	87.29	132,112	92.76	195.92	−2.04
300.00	134,115	87.24	134,100	88.96	298.73	−0.42
400.00	132,118	88.17	132,100	88.96	402.22	0.55
500.00	135,119	88.79	135,98	88.30	397.25	−20.55
600.00	133,119	88.79	133,98	88.30	397.25	−33.79
700.00	132,121	89.11	132,99	88.63	521.48	−25.50
800.00	135,121	89.11	135,102	89.61	985.49	23.19
900.00	135,122	89.75	135,100	88.96	972.43	8.048
1000.00	135,122	89.75	135,101	89.28	1154.48	15.45
1100.00	133,124	90.07	133,101	89.28	1752.78	59.34

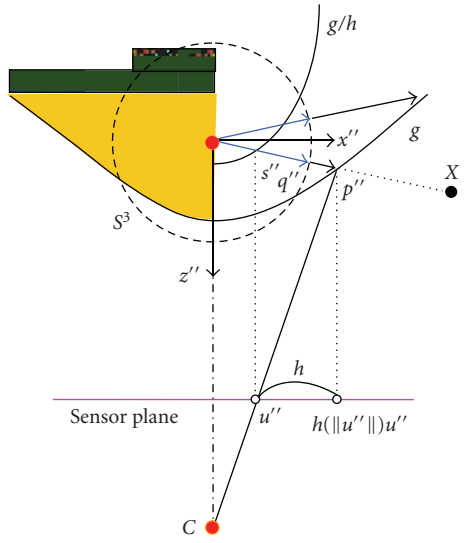

Figure 13: The mapping of a scene point X into a sensor plane to a point u'' for a hyperbolic mirror.

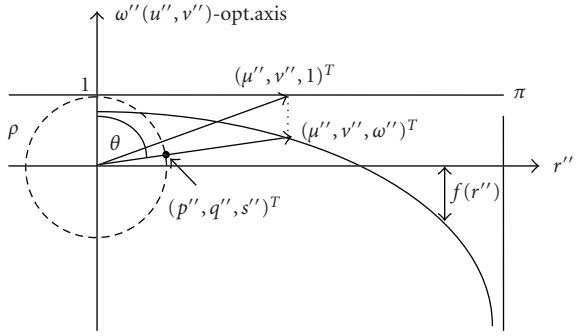

Figure 14: The point $(\mu'', \nu'', l)^T$ in the image p lane π is transformed by $f(\cdot)$ to $(\mu'', \nu'', \omega'')^T$, then normalized to $(p'', q'', s'')^T$ with unit length, and thus projected on the sphere ρ [27, 28].

3.1. Design of Hyperbolic-Shaped Mirror. Let us consider the hyperbolic-shaped mirror given in (1). An example of mirror profile obtained by this equation is shown in Figure 3

$$\frac{\left(z - \sqrt{a^2 + b^2}\right)^2}{a^2} - \frac{x^2 + y^2}{b^2} = 1. \tag{1}$$

The hyperbola is a function of two parameters a and b, but also, these parameters can be expressed by parameters c and k which determine the interfocus distance and the eccentricity, respectively. The relation between the pairs a, b and c, k is shown in (2). Figure 4 shows that the distance between the tips of the two hyperbolic napes is $2a$ while the distance between the two foci is $2c$

$$a = \frac{c}{2}\sqrt{\frac{k-2}{k}}, \qquad b = \frac{c}{2}\sqrt{\frac{2}{k}}. \tag{2}$$

By changing the values of these parameters, the hyperbola changes its shape as well as the position of the focal point. The positions of the foci of the two napes of the hyperbola determine the size of the omnidirectional sensor. The catadioptric sensor designed is used in binocular omnistereo vision sensor and is required to have large vertical angle α. Besides, image processing requires good resolution and a good vertical angle of view.

It is obvious that the azimuth field of view is 360° since the mirror is a rotational surface upon the z axis. The vertical view angle is a function of the edge radius and the vertical distance between the focal point and the containing the rim of the mirror. This relation is expressed in (3) where R_t is the radius of the mirror rim and α is the vertical view angle of the mirror

$$\alpha = \arctan\left(\frac{h}{R_i}\right) + \frac{\pi}{2}. \tag{3}$$

Therefore, R_t and h are the two parameters that bound the set of possible solutions.

The desired catadioptric sensor must possess a SVP, therefore, the pinhole of the camera model and the central

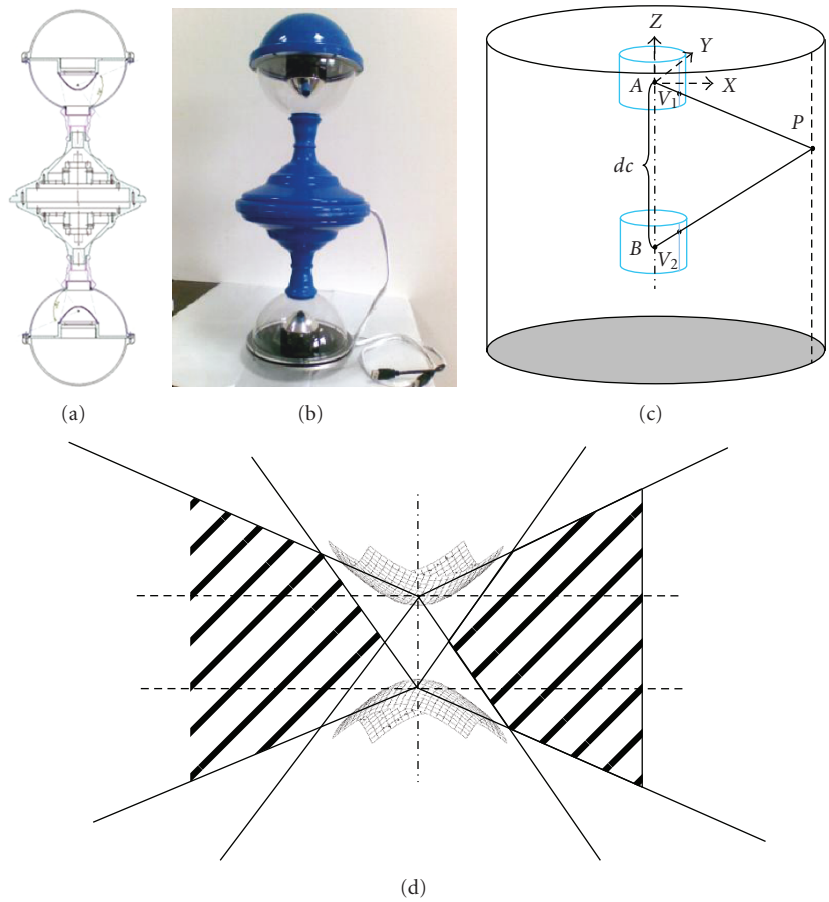

Figure 15: Vertically aligned binocular omnistereo vision sensor by face-to-face configuration (a) design drawing, (b) real product image, (c) vertically-aligned binocular omnistereo model in cylindrical surface, and (d) FOV of binocular omnistereo vision.

projection point of the mirror have to be placed at the two foci of the hyperboloid, respectively. The relation between the profile of the mirror and the intrinsic parameters of the camera, namely, the size of the CCD and the focal distance, is graphically represented in Figure 5. Here, $P_m(r_{\text{rim}}, z_{\text{rim}})$ is a point on the mirror rim, $P_i(r_i, z_i)$ is the image of the point P_m on the camera image plane, f is the focal distance of the camera and h is the vertical distance from the focal point of the mirror to its edge. Note that $z_{\text{rim}} = h$ and $z_i = -(2c + f)$. Ideally, the mirror is imaged by the camera as a disc with circular rim tangent to the borders of the image plane.

Several constraints must be satisfied during the design process of the hyperbolic mirror shape.

(i) The mirror rim must have the right shape so that the camera is able to see the point P_m. In other words, the hyperbola should not be cut below the point P_m which is the point that reflects the higher part of the desired field of view.

(ii) The points of the camera mirror rim must be on the line $\overline{P_i P_m}$ for an optimally sized image in the camera.

A study about the impact of the parameters a and b on the mirrors' profile was also conducted by T. Svoboda et al. in [10]. Svoboda underlined the impact of the ratio $k = a/b$ on the image formation when using a hyperbolic mirror.

(i) $k > b/R_t$ is the condition that the catadioptric configuration must satisfy in order to have a field of view higher than the horizon (i.e., greater than the hemisphere).

(ii) $k < (h + 2c)/R_t$ is the condition for obtaining a realizable hyperbolic mirror. This requirement implies finding the right solution of the hyperbola equation.

(iii) $k > [(h + 2c)/4cb] - [b/(h + 2c)]$ prevents focusing problems by placing the mirror top far enough from the camera).

An algorithm was developed in order to produce hyperbolic shapes according to the application requirements and taking into account the above considerations related to the mirror parameters. A mirror is presented in Figure 6 providing a vertical FOV above the horizon of 49.8 degree. If it needs a higher vertical FOV, a sharper mirror must be rebuilt.

3.2. Hyperbolic-Shaped Mirror Resolution. We assume the conventional camera has the pinhole distance u and its

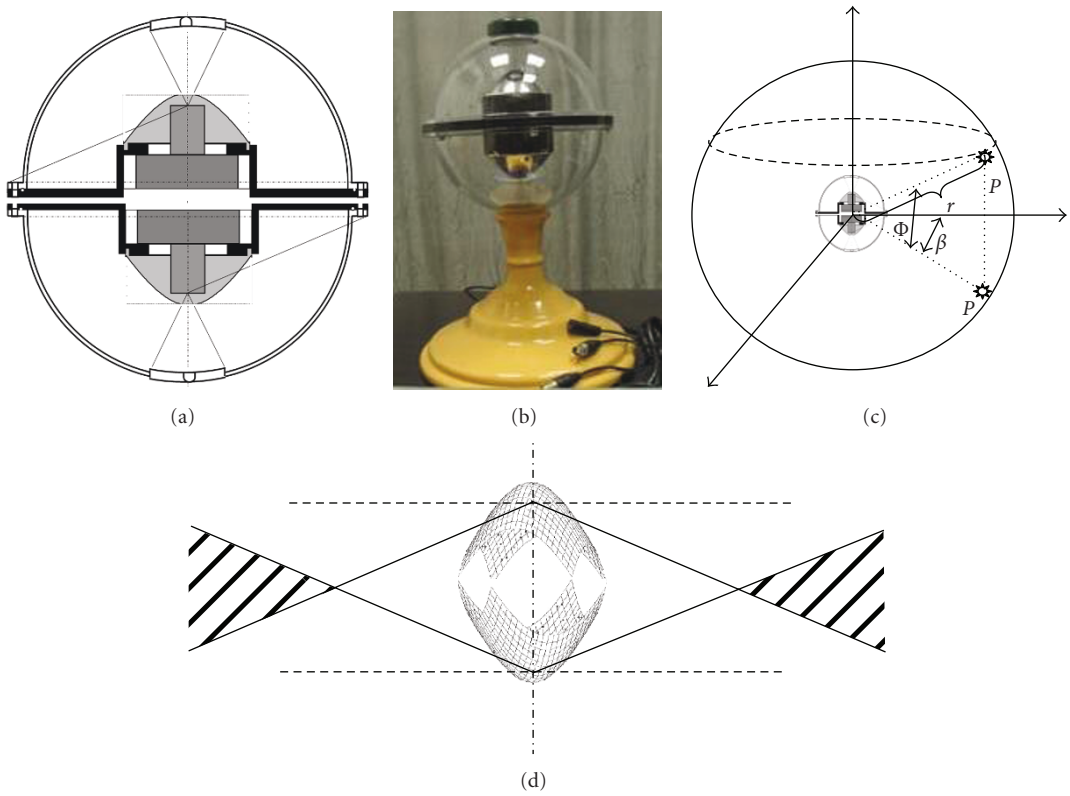

Figure 16: vertically-aligned binocular omnistereo vision sensor by back-to-back configuration (a) design drawing, (b) real product image, (c) vertically aligned binocular omnistereo model in spherical surface, and (d) FOV of binocular omnistereo vision.

optical axis is aligned with the mirror axis. The situation is depicted on the picture (Figure 7). Then, the definition of the resolution is follows. Consider an infinitesimal area dA on the image plane. If this infinitesimal pixel images an infinitesimal solid angle dv of the world, the resolution of the catadioptric sensor as a function of the point on the image plane and at the center of the infinitesimal area dA is dv/dA. The resolution of the conventional camera can be written as dw/dA. The more detailed derivation of these relations is presented in the Baker's and Nayar's work [27]. The resolution of the catadioptric camera is the resolution of conventional camera used to construct it multiplied by a factor $(r^2 + z^2)/((c - z)^2 + r^2))$. Hence, we have

$$\frac{dA}{dv} = \left[\frac{r^2 + z^2}{(c - z)^2 + r^2}\right]\frac{dA}{dw}, \tag{4}$$

where (r, z) is the point on the mirror being imaged.

The multiplication factor in (4) is the square of the distance from the point (r, z) to the effective viewpoint $v = (0, 0)$, divided by the square of the distance to the pinhole $F' = (0, c)$. Let d_v denote the distance from the viewpoint to (r, z) and d_p the distance of (r, z) from the pinhole. Then, the factor in (4) is d_v^2/d_p^2. For hyperboloid, we have $d_p - d_v = K_h$, where the constant K_h satisfies $0 < K_h < d_p$. Therefore, the factor is

$$\left[1 - \frac{K_h}{d_p}\right]^2, \tag{5}$$

Which increases as d_p increases and d_v increases. It means that the factor in (4) increases with r for the hyperbolic mirror for which it was derived. Hence, the catadioptric sensor constructed with a hyperbolic mirror and the uniform resolution conventional camera will have their highest resolution around the periphery.

Figure 8 illustrates the resolution across a radial slice of the imaging plane. The curves have been normalized with respect to magnification. It can be seen that resolution drops drastically beyond some distance from the image center.

Resolution is parameterized by the geometry of the mirror, the location of the entrance pupil, and the focal length of the lens used. Given an appropriate resolution curve, we can "fit" the right parameters in the model that most closely approximates the required curve. In the most generic setting, we could let resolution characteristics completely dictate the reflector's shape (not restricted to conic reflectors). It should, however, be noted that by fixing resolution the sensor may not maintain a single viewpoint. Depending on the application at hand, this may or may not be critical.

To design a mirror profile to match the sensor's resolution is to satisfy the Binocular Omnistereo Vision Sensor application constraints, in terms of desired image properties, such as constant angular resolution and constant vertical resolution.

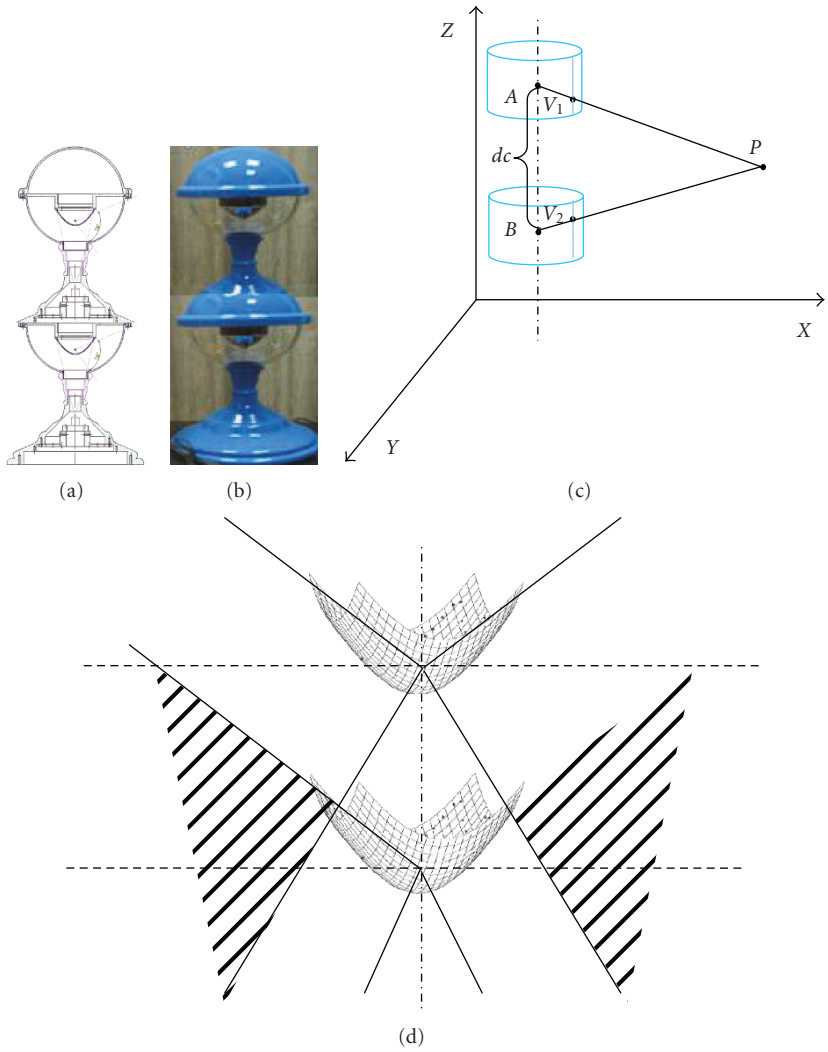

Figure 17: Vertically aligned binocular omnistereo vision sensor by face-to-back configuration (a) design drawing, (b) real product image, (c) vertically aligned binocular omnistereo model in orthogonal coordinates, and (d) FOV of binocular omnistereo vision.

3.3. Design of Constant Angular Resolution Mirror. In order to ensure that the image of transition region of two ODVSs is continuous, ODVS is designed by using the average angle. In other words, there is a linear relation between points on imaging plane and incident angle. Constant angular resolution mirror can be used to obtain spherical surface with constant resolution around the viewpoint. The spherical surface may be described in terms of r, z, the variables of interest in (6), simply as

$$r = C \times \cos(\phi), \qquad z = C \times \sin(\phi), \tag{6}$$

where C is the distance of light source P and SVP, and ϕ is the angle between the first incident light $V1$ and the spindle Z.

The design of the constant angular resolution can be reduced to the design of curve of catadioptric mirror [29]. As shown in Figure 9, the incident light $V1$ from a light source P reflects on the main mirror reflection $(t1,\ F1)$; the reflected light $V2$ reflects another time after it reflects on the secondly mirror reflection $(t2, F2)$; the reflected light $V3$ enters into the camera lens with the angle of $\theta 1$ and projected to its image on the camera.

According to imaging principle, the angle between the first incident light $V1$ and the spindle Z is ϕ, the angle between the first reflected light $V2$ and the spindle Z is $\theta 2$, the angle between the tangent through $P1$ $(t1,\ F1)$ and the spindle T is σ, and the angle between the normal and the spindle Z is ε; the angle between the secondary reflected light $V3$ and the main axis Z is $\theta 1$, the angle between the tangent through $P2$ $(t2,\ F2)$ and the spindle T is σ_1, and the angle

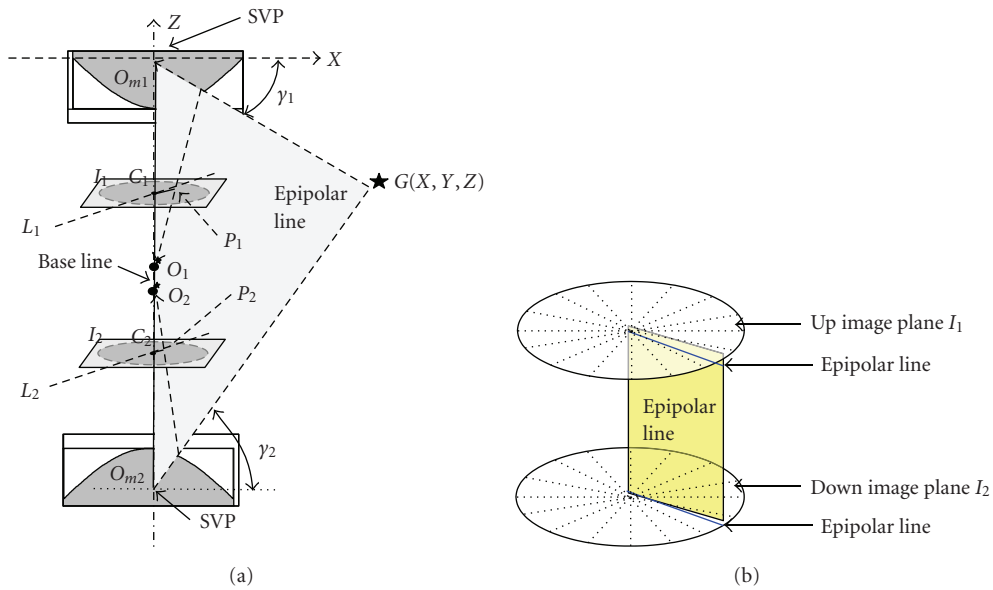

FIGURE 18: The epipolar geometry of two central catadioptric cameras with hyperbolic mirrors. (a) epipolar plane of two SVP ODVS, and (b) epipolar plane with two epipolar lines.

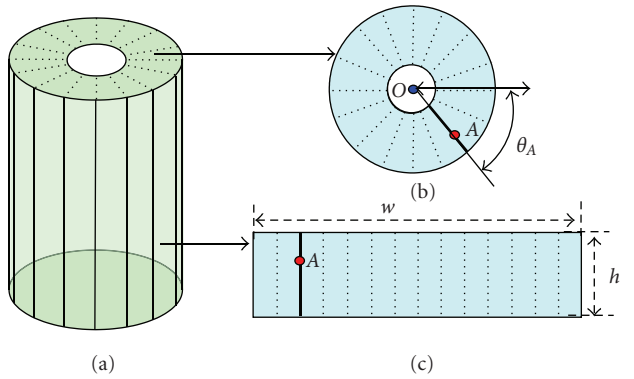

FIGURE 19: Epipolar geometry. (a) Imaging model. (b) The epipolar lines for a pair of coaxial omnidirectional images are radial lines. (c) When the images are projected onto a panorama, the epipolar lines become parallel.

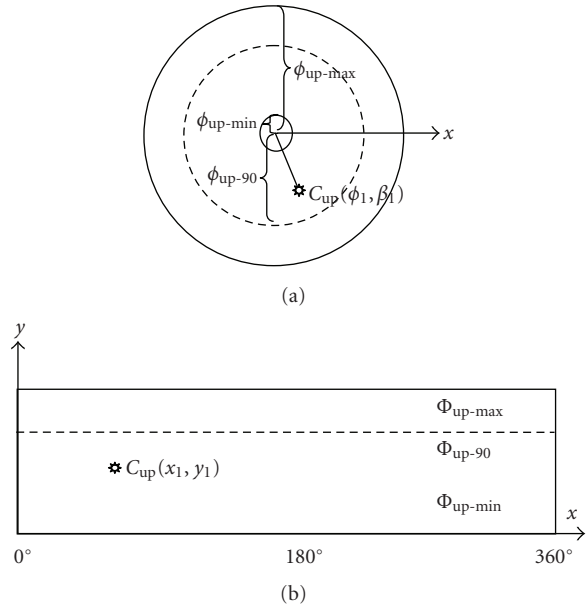

FIGURE 20: Schematic diagram of panoramic vision photo graphed by upper ODVS.

between the normal and the spindle Z is ε_1. Due to these relations, we can get

$$\begin{aligned} \sigma &= 180^\circ - \varepsilon, \\ 2\varepsilon &= \phi - \theta_2, \\ \sigma_1 &= 180^\circ - \varepsilon_1, \\ 2\varepsilon_1 &= \theta_1 - \theta_2 \end{aligned} \tag{7}$$

$$\tan\phi = \frac{t_1}{F_1(t_1 - s)}, \qquad \tan\theta_1 = \frac{t_2}{F_2}, \qquad \tan\theta_2 = \frac{t_1 - t_2}{F_2 - F_1}. \tag{8}$$

In (8), $F1$ is the firstly reflection mirror curve, $F2$ is the secondary reflection mirror curve. Using the triangular relationship and simplifying (8), we can get

$$F_1'^2 - 2\alpha F_1' - 1 = 0, \tag{9}$$

$$F_2'^2 - 2\beta F_2' - 1 = 0. \tag{10}$$

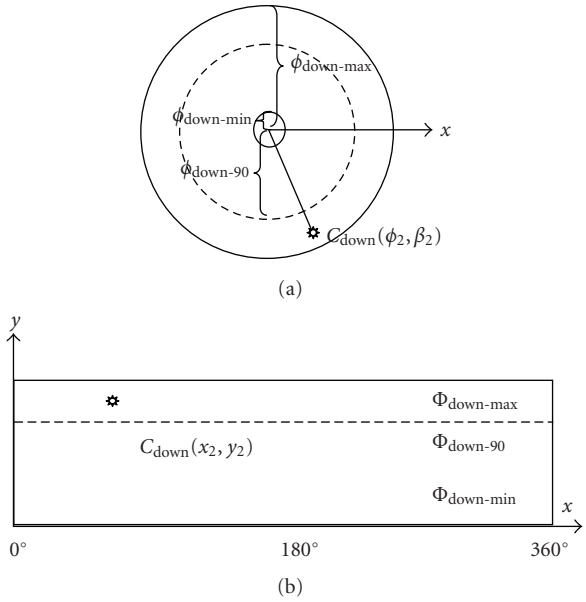

Figure 21: Schematic diagram of panoramic vision photo graphed by lower ODVS.

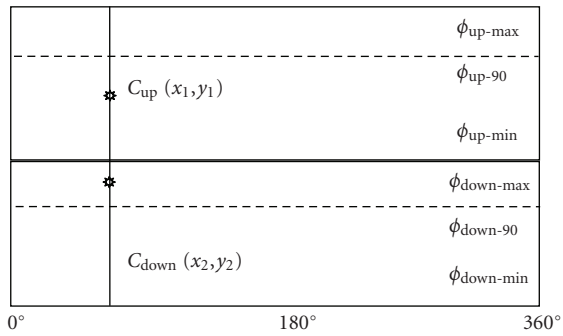

Figure 22: Image point matching for two ODVS.

Among them,

$$\alpha = \frac{(F_1 - s)(F_2 - F_1) - t_1(t_1 - t_2)}{t_1(F_2 - F_1) - (t_1 - t_2)(F_1 - s)},$$
$$\beta = \frac{t_2(t_1 - t_2) + F_2(F_2 - F_1)}{t_2(F_2 - F_1) - F_2(t_1 - t_2)}. \tag{11}$$

Solutions of (9), (10) can be

$$F_1' = \alpha \pm \sqrt{\alpha^2 + 1}, \tag{12}$$

$$F_2' = \beta \pm \beta\sqrt{\beta^2 + 1}. \tag{13}$$

Among them, F_1' is the differential of curve F_1, F_2' is the differential of curve F_2.

In order to build some certain linear relationship between a point on the image plane and the angle, it is necessary to build a linear relationship between the distance from the pixels P to the spindle Z and the angle, namely

$$\phi = a_0 \cdot P + b_0, \tag{14}$$

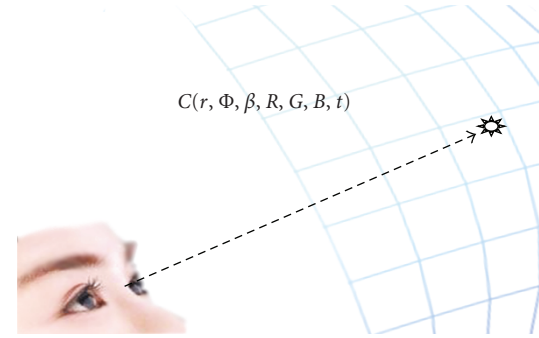

Figure 23: Imaging point expression in Gaussian reference frame coordinates.

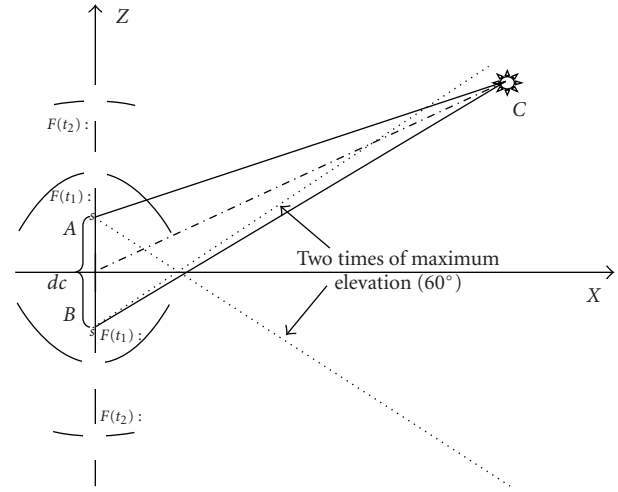

Figure 24: The measurement principle of binocular omnistereo vision sensor.

where a_0, b_0 are arbitrary parameters.

Let f represent the focal length of the camera modules, p represent the distance from the pixel point to the spindle Z, and $(t_2,\ F_2)$ represent the reflex points on the secondary reflection mirror. According to imaging principle, we have

$$P = f \cdot \frac{t_2}{F_2}. \tag{15}$$

From (8) and (9), we have

$$\phi = a_0 \cdot \left(f \cdot \frac{t_2}{F_2}\right) + b_0. \tag{16}$$

The mirror curve meeting (16) can meet the requirements of average angle resolution.

According to the principle of catadioptric, from (16), we get

$$\tan^{-1}\left(\frac{t_1}{F_1 - s}\right) = a_0 \cdot \left(f \cdot \frac{t_2}{F_2}\right) + b_0. \tag{17}$$

From (9), (10), and (17), we get the digital solutions of F_1 and F_2 through the four order Runge-Kutta algorithm (as shown in Figure 10). Thus, the firstly reflecting mirror and secondary folding mirror reflection obtained are of the constant angle resolution.

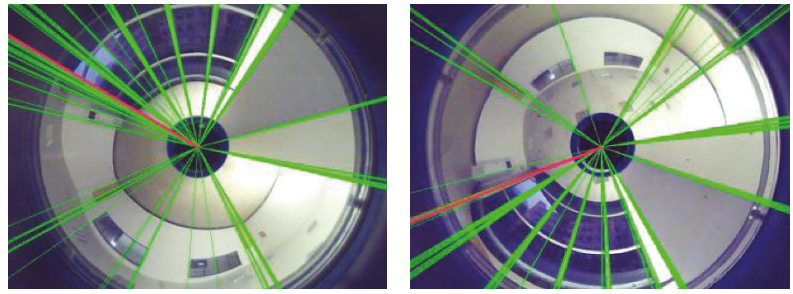

(a) (b)

Figure 25: Panoramic images, detection of reliable line, and deviation compute of epipolar lines.

Figure 26: Unwrap omnidirectional image based on epipolar match.

Figure 27: Imaging point matching for V-binocular ODVS using SIFT algorithm.

3.4. Design of Constant Vertical Resolution Mirror. This design constraint aims to achieve the goal that objects at a (prespecified) fixed distance from the camera's optical axis will always be the same size in the image and independent of its vertical coordinates. In other words, if we consider a cylinder of radius, C, around the camera optical axis, we want to ensure that ratios of distances (measured in the vertical direction along the surface of the cylinder) remain unchanged when measured in the image. Such invariance should be obtained by adequately designing the mirror profile—yielding a constant vertical resolution mirror.

As a practical example, this viewing geometry would allow reading signs or text on the surfaces of objects with minimal distortion. As another example, tracking is facilitated by reducing the amount of distortion that an image target undergoes when an object is moving in 3D. Finally, in visual navigation it helps by providing a larger degree of invariance of image landmarks with regard to the viewing geometry.

Similar to the design of constant angular resolution mirror, we can change constraints condition for (16) to get constraints (18) in constant vertical resolution [29].

$$z = a_0 \cdot \left(f \cdot \frac{t_2}{F_2} \right) + b_0. \tag{18}$$

Then, the first reflecting mirror and the second folding mirror reflection are obtained for the constant vertical resolution using the four order Runge-Kutta algorithm.

3.5. Fixed Single Viewpoint Camera Calibration. Another important property of such designed mirrors is distance sensitivity [25]. This value determines how the linear projection properties degrade for objects laying at distinct distances than those considered for the design. Since we know the geometry of the catadioptric system, we can compute the direction of light for each pixel passing through the viewpoint. In this case, single effective viewpoint permits the construction of geometrically correct panoramic images as well as perspective [27].

A camera model can be built and calibrated if the mirror surface is considered as a known revolution shape and is modeled explicitly. For instance, the reflecting surface can be a hyperboloidal placed in front of a common camera. Another way of approaching camera calibration is assuming that the pair camera-mirror possesses a SVP [25].

In order to satisfy the single viewpoint constraint, hyperboloidal omnistereo is composed of the hyperboloidal mirror and the pinhole camera in the same vertical direction, and the camera focus at the same position with hyperboloidal mirror of the virtual focus C. So, the imaging process can be divided into two steps: the conversion of mirror to the sensor plane, and the conversion of sensor plane to the image plane, as shown in Figure 12.

Every line passing through an optical center intersects the image plane in one point, so we can represent rays of the image as a set of unit vectors in R^3 such that one vector corresponds just to one image of a scene point.

Let a scene point $X = [x, y, z]^T$ be projected into $\mathbf{u}''$ in a sensor plane. Assume that the point $\mathbf{u}'' = [u'', v'']^T$

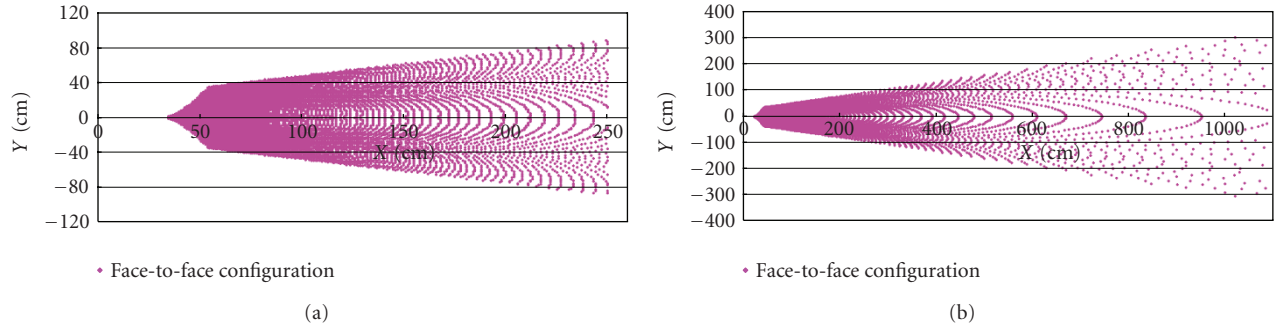

Figure 28: (a) Depth resolution for V-binocular ODVS with face-to-face configuration in 250 cm. (b) Depth resolution for V-binocular ODVS with face-to-face configuration in 1100 cm.

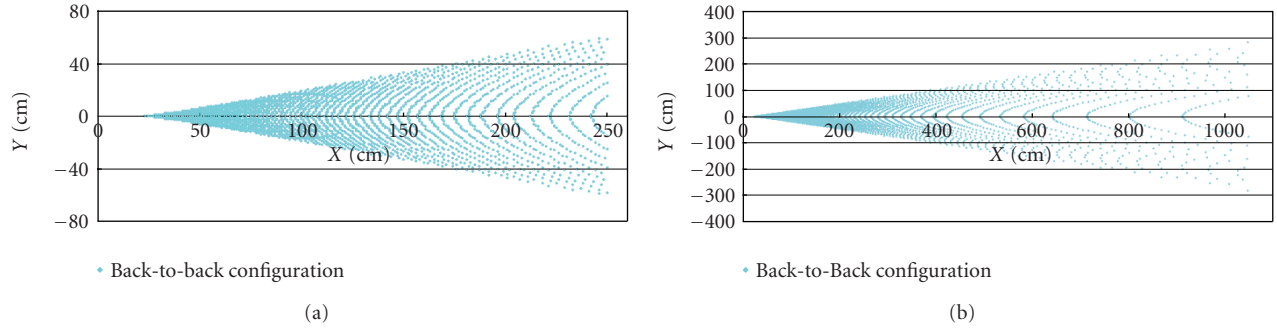

Figure 29: (a) Depth resolution for V-binocular ODVS with back-to-back configuration in 250 cm. (b) Depth resolution for V-binocular ODVS with back-to-back configuration in 1100 cm.

in the sensor plane (see Figure 12(a)) and a point $\mathbf{u}' = [u', v']^T$ in a digitized image (see Figure 12(b)) are related by an affine transformation. Thus, $\mathbf{u}'' = A\mathbf{u}' + t$, where and $A \in R^{2\times 2}$, $t \in R^{2\times 1}$. The complete image formation for omnidirectional cameras can be written as

$$\begin{aligned}\exists \alpha > 0 : \alpha \begin{bmatrix} x''^T \\ z'' \end{bmatrix} &= \alpha \begin{bmatrix} h(\|u''\|)u'' \\ g(\|u''\|) \end{bmatrix} \\ &= \alpha \begin{bmatrix} h(\|Au' + t\|)(Au' + t) \\ g(\|Au' + t\|) \end{bmatrix} = PX,\end{aligned} \tag{19}$$

where matrix X is the homogeneous coordinate of the scene point, $X = [x, y, z, l]^T \in R^4$, matrix $P \in R^{3\times 4}$ expresses perspective projection of the scene X to its digitized image $\mathbf{u}'$. The nonlinear function g defined the geometrical shape of mirror, and the nonlinear function h defined in the relation of $\mathbf{u}''$ and $h(\|\mathbf{u}''\|)\mathbf{u}''$. $\|\mathbf{u}''\|$ is the distance of image point to the center in sensor plane.

As the function g, h are the equation on the $\mathbf{u}''$, Scaramuzza et al. [30] made further analysis on perspective projection model, and proposed using a function $f = g/h$ to replace the function g, h. Then, (19) can be simplified

$$\exists \alpha > 0 : \alpha \begin{bmatrix} x'' \\ z'' \end{bmatrix} = \alpha \begin{bmatrix} u'' \\ f(\|u''\|) \end{bmatrix} = PX, \tag{20}$$

where f is rotationally symmetric with respect to the sensor axis, because both mirror profiles and pinhole camera are manufactured with micrometric precision.

To take full advantage of this rotation symmetric, and want this model to compensate for any misalignment between the focus point of the mirror and the camera optical center, Scaramuzza proposed the following Taylor polynomial form for f

$$f(||u''||) = a_0 + a_1||u''|| + a_2||u''||^2 + \cdots + a_N||u''||^N, \tag{21}$$

where the coefficients $A, t, a_0, a_1, \ldots, a_N$ and the polynomial degree N are the model parameters to be determined by the calibration. The specific methods of operation are given in the literature [31].

Establishing a two-dimensional coordinate XoZ with the focus point F, function $f = g/h$ can be described as the curve in Figures 13 and 14 mapping the vertical distance of point u'' in the sensor plane, namely, the vertical distance of the intersection point S'' and effective viewpoint f. Here, the point S'' is intersection of the vertical line of point u'' and the incident light. The angle ϕ of incident light and the z-axis holds

$$\begin{aligned}\tan\phi &= \frac{\|u''\|}{f(\|u''\|)} \\ &= \frac{\|u''\|}{a_0 + a_1\|u''\| + a_2\|u''\|^2 + \cdots + a_N\|u''\|^N}.\end{aligned} \tag{22}$$

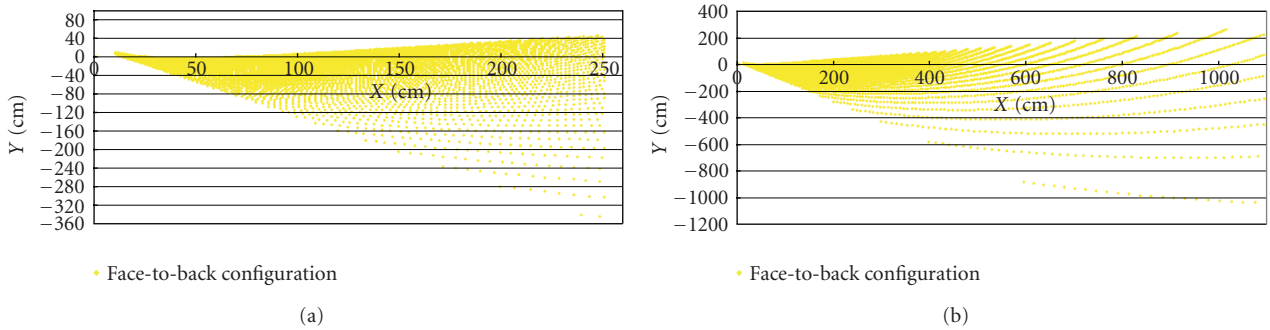

Figure 30: (a) Depth resolution for V-binocular ODVS with face-to-back configuration in 250 cm. (b) Depth resolution for V-binocular ODVS with face-to-back configuration in 1100 cm.

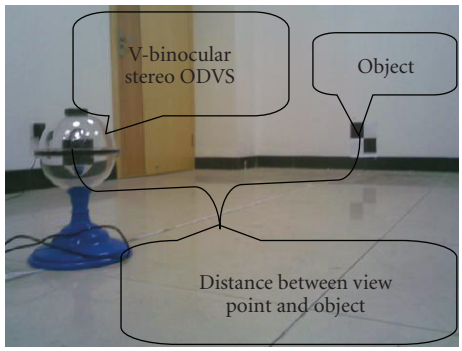

Figure 31: Experiments for measuring depth of object.

Equations (20) and (22) capture the relationship between the point u' in the digitized image and the vector P'' emanating from the optical center to a scene point X.

4. Design of Vertically Aligned Binocular Omnistereo Vision Sensor

There are some omnistereo sensors and systems. Some of the drawbacks in other omnistereo can be overcome by a vertically aligned binocular omnistereo configuration (Figures 15, 16, and 17). The depth equation of the V-binocular stereo is simply the same as a traditional perspective stereo. Previously work in V-binocular omnistereo includes the approaches using two optical omnidirectional sensors [24, 28] and using a pair of 1D scanning cameras [32]. In the later approach, high-resolution stereo pair is captured by a pair of vertically aligned 1D scan cameras. Because of the simple epipolar geometry, the depth map could be recovered during rotation in the scanning approach. Although the scanning approach cannot be applied in dynamic scenes, it is a simple and practical solution for modeling static scenes in high resolution.

4.1. Vertically Aligned Binocular Omnistereo Vision Sensor with Face-to-Face Configuration. Figure 15 shows Design drawing, Real product image, Vertically-aligned binocular omnistereo model in cylindrical surface and FOV of various vertically aligned binocular omnistereo vision sensor by face-to-face configuration. The diagonal part of the Figure 15(d) is the range of binocular stereo vision.

The face-to-face configuration with a larger range of binocular stereo range is more suitable to the mathematic geometric calculations in the cylindrical coordinate system. Furthermore, it can implement a longer baseline distance. Constant vertical resolution mirror is more appropriate for this configuration.

4.2. Vertically Aligned Binocular Omnistereo Vision Sensor with Back-to-Back Configuration. Figure 16 shows design drawing, real product image, vertically aligned binocular omnistereo model in cylindrical surface, and FOV of various vertically aligned binocular omnistereo vision sensor by back-to-back configuration. The diagonal part of the Figure 16(d) is the range of binocular stereo vision.

The face-to-face configuration with a smaller range of binocular stereo can be captured in $360° \times 360°$ global surface real-time video images and is suitable to the mathematic geometric calculations in spherical coordinate system. It has a shorter baseline distance, and is easy to be miniaturized due to its compact structure. The mirror designed with average angle resolution is more appropriate for this configuration.

4.3. Vertically Aligned Binocular Omnistereo Vision Sensor with Face-to-Back Configuration. Figure 17 shows Design drawing, Real product image, vertically aligned binocular omnistereo model in orthogonal coordinates, and FOV of various vertically aligned binocular omnistereo vision sensor by face-to-back configuration. The diagonal part of the Figure 17(d) is the range of binocular stereo vision. The range of face-to-back configuration of binocular stereo is isotropic.

As the catadioptric images are in the same direction, it may be better that hyperbolic mirrors are selected for binocular stereo catadioptric mirrors. It is more suitable for the camera measurement and the mathematic geometric calculations in the rectangular plane system. Baseline length is shorter than that of Figure 15 case, but longer than that of Figure 16 case.

(a) Sphere panoramic image (b) Unwrapped panoramic image (depth = 100 cm)

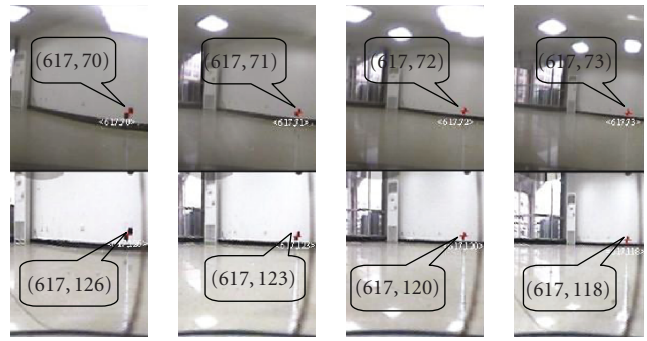

(c) Depth = 200 cm (d) Depth = 300 cm (e) Depth = 400 cm (f) Depth = 500 cm

Figure 32: Experiments for matching the object point and measuring the depth of object point.

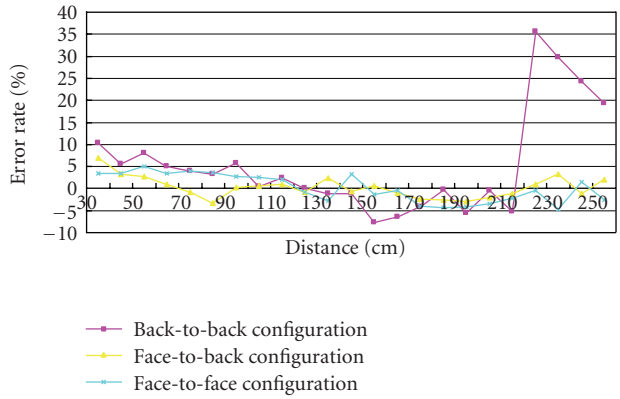

Figure 33: Depth error rate of viewing object from 30 cm to 250 cm for there V-binocular ODVS configuration.

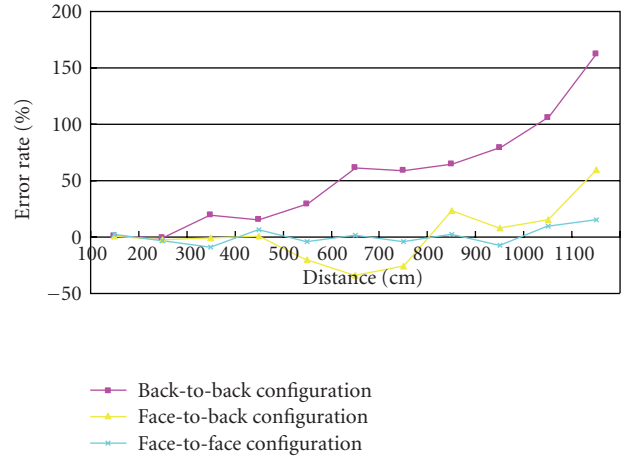

Figure 34: Depth error rate of viewing object from 100 cm to 1100 cm for there V-binocular ODVS configuration.

4.4. Epipolar Geometry. Epipolar geometry describes a geometric relationship between the positions of the corresponding points in two images acquired by central cameras [33]. Since the epipolar geometry is a property of central projection cameras, it also exists for central catadioptric cameras, for example, back-to-back configuration, see Figure 18.

(1) In Figure 18, $G(X, Y, Z)$ is an object point of three-dimensional space. Point O_{m1},O_{m2} is the focus of hyperbolic mirror. I_1,I_2 is CCD imaging plane. C_1,C_2 is the center point of image plane. P_1, P_2 is the image point of object point G. L_1 is the line through point C_1 and P_1, and L_2 is the line through point C_2 and P_2.

(2) From the Figure 18, we can see that point P_1 and P_2 is a pair of imaging points about object point G. As the points C_1,C_2,P_1, P_2 are in the epipolar plane specified by points G, O_{m1} and O_{m2}, and plane I_1 parallel to the plane I_2, then points P_1 and P_2 must be located on the line L_1 and L_2, respectively.

(3) that is, point P_1's match point, P_2, must be located on P_1's epipolar line L_2, and point P_2's match point, P_1, must be located on P_2's epipolar line L_1.

In stereo vision, the epipolar constraint is an important part (as described above). This constraint reduces the problem of finding corresponding points to a 1-D search. The epipolar constraint for catadioptric systems has been studied by [Nene and Nayar, 1998] and [10]. For hyperbolic mirror, the epipolar lines are radial lines, and corresponding points must lie on its epipolar.

Once the image of the hyperboloid is projected onto a cylinder (panoramic image), the epipolar lines become parallel. Moreover, if each image in the stereo pair is projected onto a cylinder of the same size, the epipolar lines will match up.

5. Unwrap Omnidirectional Image, Match Feature Points, and Calculate Spatial Information

5.1. Unwrap Omnidirectional Image. Omnidirectional image unwrap algorithm unwraps all omnidirectional images from ODVS. As shown in Figure 19, x-axis of image expresses azimuth angle, y-axis expresses incidence angle in this paper.

We need to separate image of central part from omnidirectional image. After that, omnidirectional image is unwrapped: the calculated step at horizontal direction in the unwrap algorithm is $\Delta\beta = 2\pi/l$; the calculated step at vertical direction in the unwrap algorithm is $\Delta m = (\phi_{\max} - \phi_{\min})/m$; in the equation, $\phi_{\max}$ is the scene lighting angle corresponding the biggest effective radius (Rmax) of the panorama relevant, and $\phi_{\min}$ is the scene lighting angle corresponding the smallest effective radius (Rmin) of the panorama relevantly. Refer to Potúček [26] for details on omnidirectional image unwrap algorithm.

The coordinate of C corresponding the original point $C(\phi, \beta)$ represented by polar coordinates is

$$x = \frac{\beta}{\Delta\beta}, \qquad y = \frac{\phi - \phi_{\min}}{\Delta m}. \tag{23}$$

In (23), $\Delta\beta$ is the calculated step in the horizontal direction, β is azimuth angle, Δm is the calculated step in the vertical direction, ϕ is the scene lighting angle corresponding the effective radius R of the panorama relevant, and $\phi_{\min}$ is the scene lighting angle corresponding the smallest effective radius (Rmin) of the panorama relevantly.

5.2. Match of Image Point. Figure 20 shows unfolded image of SVP ODVS. In unfolded image, x-axis expresses azimuth angle, and y-axis expresses incidence angle. The principle of splicing is to match the azimuth angle of two SVP ODVS, which makes the same object from two unfolded image to be on the same vertical line in splicing image. If it justifies the longitude of the two SVP ODVS when designing, it realizes the condition of bound by a line in the structure. After meeting the condition of bound by a line in the structure, the problem of searching corresponding points from the entire plane is transformed into the problem of searching corresponding points in a vertical line, which provides foundation for the rapid match between point-to-point. From the point of view of latitude, if there are certain linear relation between the incidence angle and the pixels on image plane of the SVP ODVS designed, the incidence angle of the two SVP ODVS combined can be calculated conveniently, and also we can simplify the problem of searching corresponding points in a vertical line to that in a certain area of the vertical line. As shown in (24), (e.g., back-to-back configuration)

$$180^\circ \le \phi_1 + \phi_2 \le 2\phi_{\max}. \tag{24}$$

In the equation, ϕ_1 is the incident angle of ODVS's imaging point which is underneath, ϕ_2 is the incident angle of ODVS's imaging point which is aloft, and $\phi_{\max}$ is the maximum of ODVS imaging point called elevation.

We mark the ODVS aloft as ODVSup and the ODVS underneath as ODVSdown. Assume that the object point C is in the range of the binocular vision. Its imaging point in the panorama relevant of ODVSdown is $C_{up}(\phi_1, \beta_1)$ (shown in Figure 20(a)), and its object point in the spherical launched plans is $C_{up}(x_1, y_1)$ (shown in Figure 20(b)). In the figure, $\phi_{\text{up-max}}$ shows the elevation when the incidence angle of ODVSup is biggest, $\phi_{\text{down}-90}$ shows the value when the incidence angle of ODVSup is 90°, and $\Phi_{\text{up-min}}$ shows the depression angle when the incidence angle of ODVSup is the smallest.

We can also know that object point C's imaging point in the panorama relevant of ODVSdown is $C_{down}(\phi_2, \beta_2)$ (shown in Figure 21(a)), and its object point in the spherical launched plans is $C_{down}(x_2, y_2)$ (shown in Figure 21(b)).

The incidence angle bigger than 90° is called elevation angle, while the one smaller than 90° is called depression angle. In this paper, set the incidence angle of the ODVS as elevation, so it must have some area that both of two ODVSs can reach, and that is named binocular vision scope. For the same object point in the space, if it can be seen in the binocular vision scope, it must have two image points $C_{up}(\phi_1, \beta_1)$ and $C_{down}(\phi_2, \beta_2)$ in the panorama relevant of the two ODVS which have the same azimuth angle β, that is, $\beta_1 = \beta_2$.

As a result, the X coordinate corresponding to the spherical launched plans is same too, that is, $x_1 = x_2$. So according to this principle, we can justify the azimuth angle in the spherical launched plans of two ODVS, as shown in Figure 22. Actually, Figure 22 is the mixture of Figures 20(b) and 21(b), which can realize the justifying of the azimuth angle in the spherical launched plans conveniently.

5.3. The Coordinate of Gaussian Sphere and Central Eye. Human-centered stereo omnidirectional vision has high third dimension and fidelity. We call the center of binocular vision's baseline central eye which is used to describe the information of object point $C(r, \Phi, \beta, R, G, B, t)$ in space. The meaning of each physical parameter is shown in Figure 23.

Equation (25) can be used to represent any object point in space

$$c = C(r, \Phi, \beta, R, G, B, t). \tag{25}$$

We adopt a scientific and uniform Gaussian sphere coordinate in binocular stereo vision to express all object point by using seven physical parameters. It can lay a good technology foundation for model simplification and fast calculation later. It also provides convenience for the follow-up geometric calculation.

5.4. Object Point's Spatial Information and Color Information Acquisition and Calculation. The spatial information of object point is expressed by three parameters r, Φ, and β in Gaussian sphere coordinate. Because we use central eye as the origin of Gaussian sphere coordinate, the calculation of spatial information turns into the calculation of the position relation between object point and central eye. Among them, r expresses the distance between origin O and object point. Compared to central eye, object point's longitude value is Φ and object point's latitude value is β. According to the principle of binocular vision, we can estimate the object point's depth information, as shown in Figure 9.

According to the imaging principle of binocular vision, we can get the distance between object point and viewpoint that is depth of field only if we obtain the incidence angle of object point at two ODVSs ϕ_1 and ϕ_2. Because two ODVSs are composed with Back-to-Back configuration, ϕ_1 and ϕ_2 can be calculated by

$$\begin{aligned}\phi_1 &= \phi_{\min} + \frac{(\phi_{\max} - \phi_{\min})}{m \cdot (m - y_1)},\\ \phi_2 &= \phi_{\min} + \frac{(\phi_{\max} - \phi_{\min})}{m \cdot y_2}.\end{aligned} \tag{26}$$

In the equation, m is the height of unwrapped image. y_1, y_2 is match point's y-axis in two unwrapped images. $\phi_{\min}$ is the minimum incidence angle. $\phi_{\max}$ is the maximum incidence angle.

According to the triangular relationship, we can get the distance r between origin O and object point C

$$\begin{aligned} r = \overline{OC} &= \sqrt{\overline{AC}^2 + \left(\frac{dc}{2}\right)^2 - 2\overline{AC}\left(\frac{dc}{2}\right)\cos A}\\ &= \sqrt{\left[\frac{dc}{\sin(B+A)} \cdot \sin B\right]^2 + \left(\frac{dc}{2}\right)^2 - \frac{dc^2}{\sin(B+A)} \cdot \sin B \cos A}\\ &= \sqrt{\left[\frac{dc}{\sin(\phi_1+\phi_2)} \cdot \sin\phi_1\right]^2 + \left(\frac{dc}{2}\right)^2 - \frac{dc^2}{\sin(\phi_1+\phi_2)} \cdot \mathfrak{A}}, \end{aligned} \tag{27}$$

where $\mathfrak{A}$ denotes $\sin\phi_1 \cos\phi_2$.

In the equation, $\angle A = 180 - \phi_2, \angle B = 180 - \phi_1$, and dc is the distance between ODVSup's viewpoint and ODVSdown's viewpoint.

The angle Φ can be calculated by (28):

$$\Phi = \arcsin\left(\frac{dc}{2r}\sin\phi_2\right) + \phi_2 - 180^\circ. \tag{28}$$

Φ is the incidence angle of object point; dc is the distance between point A and point B in binocular system; r is the distance between feature point and central eye; ϕ_2 is the incidence angle of ODVSup.

Another parameter of object point β can choose any one from two ODVS's azimuth angle. t is the time from computer system.

The average value of each color components R, G, and B from matching points of two unwrapped images is adopted in the calculation of color information as central eye's color-coding. First, we obtain color components R_{ODVS1}, R_{ODVS2}, G_{ODVS1}, G_{ODVS2}, B_{ODVS1}, and B_{ODVS2} and from matching points of two unwrapped images, then calculate the average value of each color components as central eye's color coding. The equation is shown as follows:

$$\begin{aligned} R &= \frac{R_{\text{ODVS1}} + R_{\text{ODVS2}}}{2},\\ G &= \frac{G_{\text{ODVS1}} + G_{\text{ODVS2}}}{2},\\ B &= \frac{B_{\text{ODVS1}} + B_{\text{ODVS2}}}{2}. \end{aligned} \tag{29}$$

In the equation, R is the average value of red component, R_{ODVS1} is red component of ODVS one, R_{ODVS2} is red component of ODVS two. G is the average value of green component, G_{ODVS1} is green component of ODVS one, G_{ODVS2} is green component of ODVS two. B is the average value of blue component, B_{ODVS1} is green component of ODVS one, B_{ODVS2} is blue component of ODVS two. The value range of them are 0∼255.

5.5. Depth Accuracy. The vertically aligned binocular omnistereo systems have two viewpoints and fixed baseline. For the stereo matching between the two converted panoramic views, any conventional algorithms are applicable. Once correspondence between image points is established, depth computation in both spherical and cylindrical panorama is straightforward by simple triangulation in (27). In addition, the depth resolution mainly depends on camera resolution, the length of baseline and binocular omnistereo vision sensor configuration

$$\partial r = f\left(\frac{r^2}{dc}\right)\partial\phi, \tag{30}$$

where r is the distance between viewing object and binocular omnistereo vision sensor, dc is the length of baseline, and $\partial\phi$ is similar to the camera resolution. It seems that larger baseline and higher camera resolution will get better depth accuracy. Therefore, depth estimation error is proportional to the square of the distance between viewing object and binocular omnistereo vision sensor. The depth accuracy of the V-binocular omnistereo is isotropic in all directions, and the epipolar lines are simply vertical lines in omnidirectional image. More detail of the depth resolution and error analysis can be found in references [34, 35].

6. Experiment Results

According to the above idea, we have developed three V-binocular stereo ODVS types as shown in Figures 15(b), 16(b), and 17(b). The video information obtained from binocular stereo ODVSs are transmitted through two USB interfaces to computer, which processes the image and matches the object point, and calculates the distance of object point. Figure 25 shows the panoramic images obtained by V-binocular omnidirectional vision sensor shown in Figure 15(b), where image resolution is 640 × 480 pixels.

6.1. Epipolar Plane with Two Epipolar Lines. In order to verify the good characteristic on 3D matching of the device, in this paper, we use SIFT (scale-invariant feature transform) feature matching algorithm [36] to match the feature points for Figure 26 and obtain the results shown in Figure 27, in which all the connections of the matching points are almost parallel. In other words, it is feasible to match the feature points got from the unwrap image on the line of the connections, and, after fixing the device, use binocular ODVS to demarcate processing. Then, we can get the position of these matched line and only need to find match points on the matched line in later matching processes, which greatly reduces the complexity of the matching.

6.2. Match of Image Point. The two sensor planes formed by vertically aligned binocular omnistereo vision sensor exist a parallel error and a coaxial error, which are shown in Figure 27. Actually, match lines of all image points is not always in verticality. In other words, the same image point in the two image planes may be not in the same epipolar plane, in despite of unwrap omnidirectional image based on epipolar match, shown as Figure 26. To decrease matching error, we use normalized cross-correlation arithmetic to match feature points from up and down panoramic images, based on feature point which has same brightness in neighbor window area, shown as

$$\text{Corr} = \frac{\sum_{j=-N/2}^{N/2}\sum_{i=-M/2}^{M/2}\sum_{[r,g,b]}\{(\mathcal{A})\cdot(\mathcal{B})\}}{\sqrt{\sum_{j=-N/2}^{N/2}\sum_{i=-M/2}^{M/2}\sum_{[r,g,b]}(\mathcal{A})^2\cdot\sum_{j=-N/2}^{N/2}\sum_{i=-M/2}^{M/2}\sum_{[r,g,b]}(\mathcal{B})^2}},$$
$$\mathcal{A} = C_{\text{down}}(x_2+i, y_2+j) - \overline{C_{\text{down}}[r,g,b]},$$
$$\mathcal{B} = C_{\text{up}}(x_1+i, y_1+j) - \overline{C_{\text{up}}[r,g,b]}, \tag{31}$$

where N and M are the size of the neighbor window area. $C_{\text{up}}(x_1, y_1)$ is the brightness of feature point $I_r(x_1, y_1)$ in up panoramic image. $C_{\text{down}}(x_2, y_2)$ is the brightness of searching feature point in down panoramic image, shown as Figure 22

$$\overline{C_{\text{down}}[r,g,b]} = \sum_{j=-N/2}^{N/2}\sum_{i=-M/2}^{M/2} C_{\text{down}}[r,g,b](x_2+i, y_2+j),$$
$$\overline{C_{\text{up}}[r,g,b]} = \sum_{j=-N/2}^{N/2}\sum_{i=-M/2}^{M/2} C_{\text{up}}[r,g,b](x_1+i, y_1+j). \tag{32}$$

If the Corr of feature point $I_s(x_2, y_2)$ calculated by (28) is higher than threshold of normalized cross-correlation, this point can be the search matching feature point. In this paper, we adopt the feature point $I_r(x_1, y_1)$ in up panoramic image to search the cross-correlation feature point $I_s(x_2, y_2)$ in down panoramic image. As matching feature point must be near to its epipolar plane, the value of N is used to 6 pixels, and the value of M is determined by the image range of binocular omnistereo vision.

6.3. Measuring Depth of Viewing Object. Once the correspondence between image points has been established, depth measurement in cylindrical panorama is straightforward by simple triangulation (27) and (28). Figures 28, 29, and 30 show a sampling of depth resolution in three kinds of FOV of Binocular Omnistereo Vision. The sampling is obtained by computing depth for every possible pair of image correspondences.

In there figure, each point represents the estimated position calculated by all the possible pair of image correspondence in a single epipolar plane, the coordinate (0, 0) expresses the position of "central eye". These instances are generated with the three configurations of V-binocular ODVS, and the parameters of each are given in above.

In order to get better depth accuracy range for special application requirements, we carry out experiments for measuring depth of viewing object using three V-binocular stereo ODVS types, that is, back-to-back configuration, face-to-face configuration, and face-to-back configuration. One of the experiment devices is shown in Figure 31 (e.g., back-to-back configuration).

The panoramic images obtained from binocular stereo ODVS are transmited to computer through two USBs. Then, the computer processes the images, matches the object point, and measures the depth of object point. Figure 32 is the panoramic image of both the above frame and the below frame graphed by V-binocular stereo ODVS with back-to-back configuration, in which sphere panoramic image resolution is 640 ∗ 480 pixels and unwrapped panoramic image resolution is 1280 ∗ 200 pixels. The experiments of measuring depth between viewing object (in red cross mark) and central eye (origin O) carried out by using the binocular stereo ODVS experiment device, from short distance to long distance, respectively. Figure 31 shows parts of experiments for matching the object point and measuring the depth of object point. The software is developed by Java and runs on Windows XP.

Experiment results of measuring depth between view point and object from 30 cm to 250 cm and 100 cm to 1100 cm are presented in Tables 2 and 3, respectively, which uses V-binocular ODVS with face-to-face configuration and chooses baseline length in Figure 15(b) as 40.58 cm. Experiment resluts of measuring depth between view point and object from 30 cm to 250 cm and 100 cm to 1100 cm are presented in Tables 4 and 5, respectively, which uses V-binocular ODVS with back-to-back configuration and chooses baseline length in Figure 16(b) as 9.80 cm. And experiment resluts of measuring depth between view point and object from 30 cm to 250 cm and 100 cm to 1100 cm are presented in Tables 6 and 7, respectively, which uses V-binocular ODVS with face-to-back configuration and chooses baseline length in Figure 17(b) as 18.70 cm.

The depth errors of viewing object from 30 cm to 250 cm and 100 cm to 1100 cm for V-binocular ODVS with face-to-face, back-to-back, and face-to-back configuration are shown in Figures 33 and 34, respectively. These results indicate that the measured value of short distance measuring is close to the actual value. This is because the closer to the center of stereo ODVS, the more accurate of the measuring point's incidence angle. From these figures, noting V-binocular ODVS with face-to-face configuration has the longest baseline length, we are aware that this configuration can get high depth measuring accuracy. In addition, the farther the target object is, the larger the baseline should be.

Now, we move on to analyze errors. According to the principle of binocular stereo vision, the position of object can be measured exactly. But the image is not continuous when it is obtained by imaging unit; that is, the image is discrete data which takes pixel as a unit. There is minimum resolution ratio error in measurement, because of the camera's resolution. This problem can be alleviated by using high resolution camera.

According to results of measurement, depth-estimation error will increase with the measuring distance enlarge. The reason is that, when measuring distance increases, the measuring point's incidence angle on two ODVS, that is, ϕ_1 and ϕ_2, becomes small and tends to 90°, which makes the distance from target object r of (30) very sensitive to the change of incidence angle.

7. Conclusion

In this paper, a novel dynamic omnistereo approach is presented, in which viewpoints of two omnidirectional cameras can form the optimal stereo configuration for localizing moving objects. Further extension is made to the concept of omnidirectional imaging from viewer-centered to object centered representation, thus allowing building omnidirectional models of large objects or even our planet. Numerical analysis is conducted on omnidirectional representation, epipolar geometry, and depth error character, which helps for the research and applications of omnidirectional stereo vision.

In the study, we conduct comparative evaluation of ODVS which are classified according to five criteria: the cabrication technology, the resolution, the SVP property, the VFOV property, and isotropy. Each category is explained and accompanied with several examples of real ODVSs with detailed descriptions. Besides, comparative evaluation of Binocular Omnistereo Vision Sensor (BOSVS) is also presented, which are classified according to five criterias: FOV of the BOSVSs, epipolar geometry, matching the image point, depth accuracy, and coordinate system for each type of BOSVSs in 3D calculations. The classification parameters and details of each type of ODVSs and BOSVSs bring valuable guidelines for the choice of ODVS or BOSVS depending on the application requirements.

Stereovision has always been an important issue of computer vision and video measurement, the benefits of the binocular omnistereo vision sensor-based stereovision measurement device developed by this work are mainly manifested in the following.

(1) Capturing the $360° * 360°$ omnidirectional 3D video images in real time and getting the panoramic images of the entire monitoring sphere through geometric calculation. Additionally, the tracked monitoring objects will not disappear from the camera.

(2) Designing the ODVS with constant angular resolution, constant vertical resolution and hyperbolic type, which can get images with no distortion and thus helps to solve the problems existing in catadioptric ODVS. Providing a complete theoretical system and model for the realization of real time tracking of fast-moving targets in large space.

(3) Proposing a new omnidirectional binocular vision. In the overlapping vision region of the two ODVS, binocular omnistereo vision sensor has the real-time perceiving, fusion faculty, and stereo feeling.

(4) Each ODVS with SVP constituting the binocular omnistereo vision sensor is designed with constant angular resolution, constant vertical resolution, and hyperbolic type, and both of the cameras employ the same criteria, which makes our device capable of achieving truly symmetry and capturing real time video image under the spherical coordinates, cylindrical coordinates, and orthogonal coordinates, respectively. As a result, we can realize point-to-point match rapidly, which gives a great convenience for the following 3D image processing.

(5) The complicated calibration work is no longer needed. Feature extraction is very convenient, and rapid 3D image matching can be achieved.

(6) There is no fixed focal length problem any more, as ODVS is developed with catadioptric technology: the image clarity is the same in any region.

(7) Double catadioptric imaging technology is employed which makes the implementation of small or echo micro device easier.

(8) Adopts a kind of uniform coordinates at the image gathering, 3D matching, 3D image reconstruction, and 3D objects measuring are much easier. The

device designed and developed can be widely used in industrial inspection, military reconnaissance, geographical surveying, medical cosmetic surgery, bone orthopedics, cultural reproduction, criminal evidence, security identification, air navigation, robot vision, mold rapid prototyping, virtual reality, animated films, games, and other application areas.

In the near future, we will investigate active omnistereo image by using stereo structure light produced by LED (Light Emitting Diode) or laser radiation device.

Acknowledgments

This project is supported by National Natural Science Foundation of China under Grant no. 61070134, 60873228 and by Key Science and Technology Project of Zhejiang Province of China under Grant no. 2009C14033.

References

[1] S. Baker and S. K. Nayar, "A theory of catadioptric image formation," in *Proceedings of the IEEE 6th International Conference on Computer Vision (ICCV '98)*, pp. 35–42, January 1998.

[2] J. S. Chahl and M. V. Srinivasan, "Reflective surfaces for panoramic imaging," *Applied Optics*, vol. 36, no. 31, pp. 8275–8285, 1997.

[3] T. L. Conroy and J. B. Moore, "Resolution invariant surfaces for panoramic vision systems," in *Proceedings of the IEEE 7th International Conference on Computer Vision (ICCV '99)*, pp. 392–397, September 1999.

[4] C. Deccó, J. Gaspar, N. Winters, and J. Santos-Victor, "Omniviews mirror design and software tools," Tech. Rep., Omniviews deliverable DI-3, September 2001, http://www.isr.ist.utl.pt/labs/vislab/.

[5] J. Gaspar, N. Winters, and J. Santos-Victor, "Vision-based navigation and environmental representations with an omnidirectional camera," *IEEE Transactions on Robotics and Automation*, vol. 16, no. 6, pp. 890–898, 2000.

[6] C. Geyer and K. Daniilidis, "A unifying theory for central panoramic systems and practical applications," in *Proceedings of the European Conference on Computer Vision (ECCV '00)*, vol. 2, pp. 445–461, June 2000.

[7] R. A. Hicks and R. Bajcsy, "Catadioptric sensors that approximate wide-angle perspective projections," in *Proceedings of the IEEE Workshop on Omnidirectional Vision (OMNIVIS '00)*, vol. 1, pp. 97–103, June 2000.

[8] F. Marchese and D. Sorrenti, "Omni-directional vision with a multi-part mirror," in *Proceedings of the 4th International Workshop on Robocup*, pp. 289–298, 2000.

[9] S. K. Nayar, "Catadioptric omnidirectional camera," in *Proceedings of the IEEE Computer Society Conference on Computer Vision and Pattern Recognition (CVPR '97)*, pp. 482–488, San Juan, Puerto Rico, USA, June 1997.

[10] T. Svoboda, T. Pajdla, and V. Hlavác, "Epipolar geometry for panoramic cameras," in *Proceedings of the European Conference on Computer Vision (ECCV '98)*, pp. 218–231, Freiburg, Germany, July 1998.

[11] K. Yamazawa, Y. Yagi, and M. Yachida, "Obstacle detection with omnidirectional image sensor HyperOmni vision," in *Proceedings of the IEEE International Conference on Robotics and Automation (ICRA '95)*, pp. 1062–1067, May 1995.

[12] B. Mičušík and T. Pajdla, "Autocalibration & 3D reconstruction with non-central catadioptric cameras," in *Proceedings of the IEEE Computer Society Conference on Computer Vision and Pattern Recognition (CVPR '04)*, vol. 1, pp. 58–65, July 2004.

[13] P. Doubek and T. Svoboda, "Reliable 3D reconstruction from a few catadioptric images," in *Proceedings of the IEEE Workshop on Omnidirectional Vision (OMNIVIS '02)*, pp. 71–78, 2002.

[14] P. Sturm, "A method for 3D reconstruction of piecewise planar objects from single panoramic images," in *Proceedings of the*

IEEE Workshop on Omnidirectional Vision (OMNIVIS '00), pp. 119–126, 2000.

[15] G.-B. Kim and S.-C. Chung, "An accurate and robust stereo matching algorithm with variable windows for 3D measurements," *Mechatronics*, vol. 14, no. 6, pp. 715–735, 2004.

[16] Q. Yang et al., "3D visual new method based on the edge of the match," *Instrumentation Journal*, vol. 22, no. 3, pp. 255–256, 2001.

[17] Z. Xunjie and L. Chengjin, "The key technology of real-time distance measurement by using binocular stereo system," *Laser and Infrared*, vol. 36, no. 9, pp. 874–877, 2006.

[18] S. You et al., "Stereo vision research and progress," *Chinese Journal of Graphic Images*, vol. 2, no. 1, pp. 17–23, 1997.

[19] Y.-P. Tang, Y.-J. Ye, Y.-H. Zhu, and X.-K. Gu, "Research on intelligent omni-directional vision sensors and their applications," *Chinese Journal of Sensors and Actuators*, vol. 20, no. 6, pp. 1316–1320, 2007.

[20] F. Zhou et al., "Field calibration technology based on binocular visual sensor," *Instrumentation Journal*, vol. 21, no. 2, pp. 1316–1320, 2000.

[21] Q. Mao-lin, "Camera calibration summary in computer visual," *Journal of Automation*, vol. 26, no. 1, pp. 43–55, 2000.

[22] H. Hirschmüller, P. R. Innocent, and J. Garibaldi, "Real-time correlation-based stereo vision with reduced border errors," *International Journal of Computer Vision*, vol. 47, no. 1–3, pp. 229–246, 2002.

[23] Y. Tang, "Omni directional vision sensors without dead angle," Chinese Patent no. 200710066757.0, 2007.

[24] J. Gluckman, S. K. Nayar, and K. Thorek, "Real-time omnidirectional and panoramic stereo," in *Proceedings of DARPA Image Understanding Workshop*, pp. 299–303, November 1998.

[25] R. Orghidan, *Catadioptric Stereo Based on Structured Light Projection*, Universitat de Girona, Catalonia, Spain, 2005.

[26] I. Potúček, *Omnidirectional Image Processing for Human Detection and Tracking*, Brno University of Technology, 2006.

[27] S. Barker and S. K. Nayar, "Single viewpoint catadioptric cameras," in *Panoramic Imaging: Sensors, Theory, and Application*, R. Benosman and S. B. Kang, Eds., 2001.

[28] B. Mičušik and T. Pajdla, "Estimation of omnidirectional camera model from epipolar geometry," in *Proceedings of the IEEE Computer Society Conference on Computer Vision and Pattern Recognition (CVPR '03)*, pp. 485–490, June 2003.

[29] J. Gaspar, C. Deccó, J. Okamoto Jr., and J. Santos, "Constant resolution omnidirectional cameras," in *Proceedings of Workshop on Omni-Directional Vision (OMNIVIS '02)*, Copenhagen, Denmark, June 2002.

[30] D. Scaramuzza, A. Martinelli, and Siegwart, "A toolbox for easy calibrating omnidirectional camera," in *Proceeding of the IEEE International Conference on Intelligent Robots and Systems*, pp. 27–34, Beijing, China, 2006.

[31] D. Scaramuzza, "Omnidirectional camera and calibration toolbox for matlab," March 2009, Google for "OCAMCALIB".

[32] K. G. Konolige and R. C. Bolles, "Extra set of eyes," in *Proceedings of DARPA Image Understanding Workshop*, vol. 1, pp. 25–32, 1998.

[33] T. Svoboda and T. Pajdla, "Epipolar geometry for central catadioptric cameras," *International Journal of Computer Vision*, vol. 49, no. 1, pp. 23–37, 2002.

[34] Z. Zhu, "Omnidirectional stereo vision," in *Proceedings of the 10th IEEE Workshop on Omnidirectional Vision (ICAR '01)*, pp. 22–25, Budapest, Hungary, August 2001.

[35] G. Jang, S. Kim, and I. Kweon, "Single camera catadioptric stereo system," in *Proceedings of the 6th Workshop on Omnidirectional Vision, Camera Networks and Non-Classical Cameras (OMNIVIS/ICCV '05)*, Beijing, China, October 2005.

[36] Y. Ke and R. Sukthankar, "PCA-SIFT: a more distinctive representation for local image descriptors," in *Proceedings of the IEEE Computer Society Conference on Computer Vision and Pattern Recognition (CVPR '04)*, vol. 2, pp. 506–513, July 2004.